UNITED NATIONS EDUCATIONAL, SCIENTIFIC AND CULTURAL ORGANIZATION
INTERNATIONAL ATOMIC ENERGY AGENCY
INTERNATIONAL CENTRE FOR THEORETICAL PHYSICS
I.C.T.P., P.O. BOX 586, 34100 TRIESTE, ITALY, CABLE: CENTRATOM TRIESTE

H4.SMR/1013-34

SCHOOL ON THE USE OF SYNCHROTRON RADIATION
IN SCIENCE AND TECHNOLOGY:
*"John Fuggle Memorial"*

3 November - 5 December 1997

*Miramare - Trieste, Italy*

---

# *Inelastic X-Ray Scattering II*

**Michael Krisch**
**European Synchrotron Radiation Facility**
**Grenoble, France**

# Inelastic X-Ray Scattering

## 2. IXS from Electronic Excitations

Michael Krisch
*European Synchrotron Radiation Facility*
*BP 220*
*F-38043 Grenoble Cedex*
*France*

A) Introduction and experimental principles

B) Resonant inelastic x-ray scattering

1) Theoretical background

2) Examples

- $Gd_3Ga_5O_{12}$, $Er_2O_3$, $RE_2Fe_{14}B$ (RE $L_3$ edge)

- $Gd_3Fe_5O_{12}$ (Fe K edge)
- $CsNi[Cr(CN)_6]$ (Ni K edge)
- Mn compounds (Mn K-edge)

- Gd metal, circular polarized x-rays (Gd $L_3$ edge)
- Fe metal, circular polarized x-rays (Fe $L_{2,3}$ edge)

- NiO (Ni K edge)

C) X-ray Raman scattering from low Z materials

1) Theoretical background

2) Examples

- Li K-edge
- Diamond
- Be and Graphite

D) Summary

# Inelastic X-ray Scattering

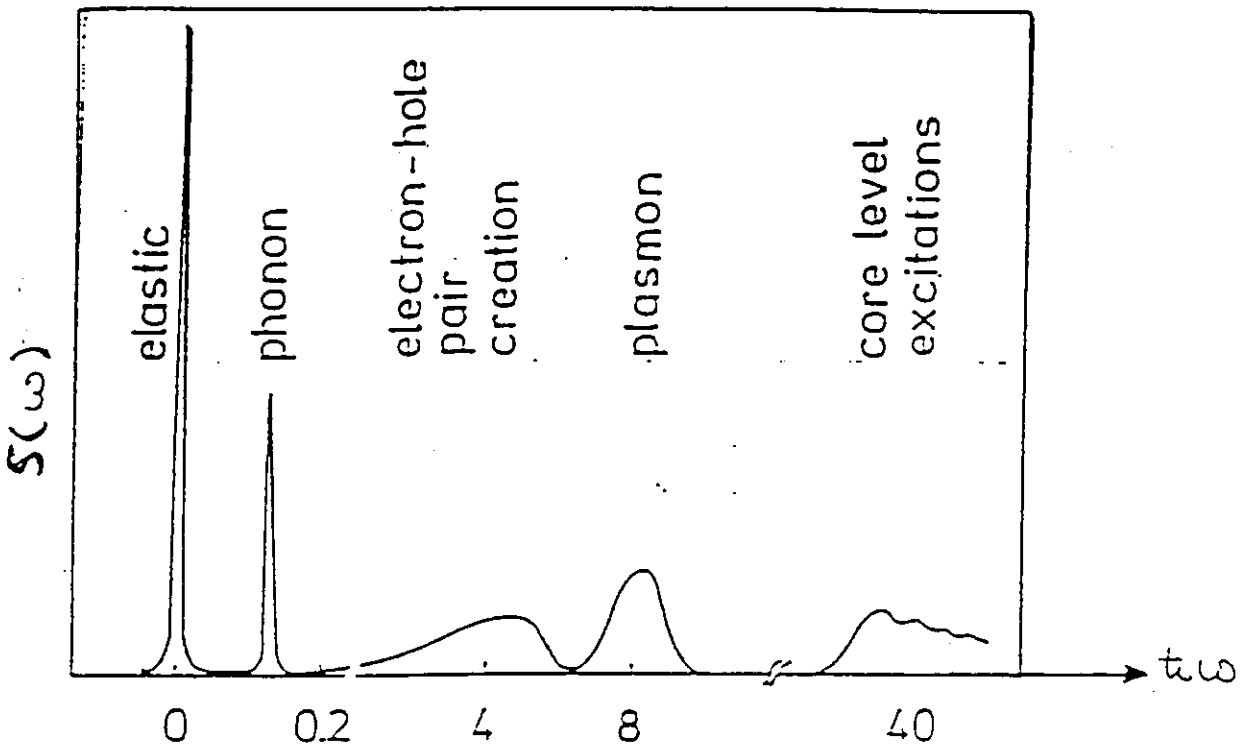


1) Collective ion excitations: $qd \approx 1$ (d: interionic distance); $\hbar\omega$: phonon energy

2) Valence electron excitations: $qr_c \approx 1$ ($r_c$: interparticle distance); $\hbar\omega$: free-electron plasma frequency

3) Inner shell excitations: $qa < 1$ (a: inner electron shell radius); $\hbar\omega$: electron binding energy

4) Compton scattering: $qr_c >> 1$; $\hbar\omega >>$ binding energy

5) Resonant Raman Scattering: $\hbar\omega_1 \sim E_{abs}$, $\hbar\omega_2 \sim E_{fl}$

# Application versus experimental needs

Inelastic x-ray scattering is a weak process:

=> extract as many photons of the desired energy as possible out of the source. (Monochromator)

=> energy analysis + collect some solid angle $\Omega$. (Analyser)

Tunability of the momentum transfer.

Selection of the polarization.

1) Collective ion excitations (phonons):

$\hbar\omega_1$: 10 - 20 keV
$\Delta\hbar\omega$: 1-10 meV

2) Valence electron excitations:

$\hbar\omega_1$: 10 keV
$\Delta\hbar\omega$: 0.3 - 3 eV

3) Non-resonant Raman scattering

$\hbar\omega_1$: 10 keV
$\Delta\hbar\omega$: 1 eV -> (0.1 eV) K-hole lifetime of light elements

4) Resonant Raman scattering:

$\hbar\omega_1$: 0.5-15 keV tunable to K-,L and M-edges of interest
$\Delta\hbar\omega$: 0.1 -1 eV ≈ lifetime of final state core-hole

## DOUBLE-CRYSTAL MONO + FOCUSING ELEMENT

TOP VIEW

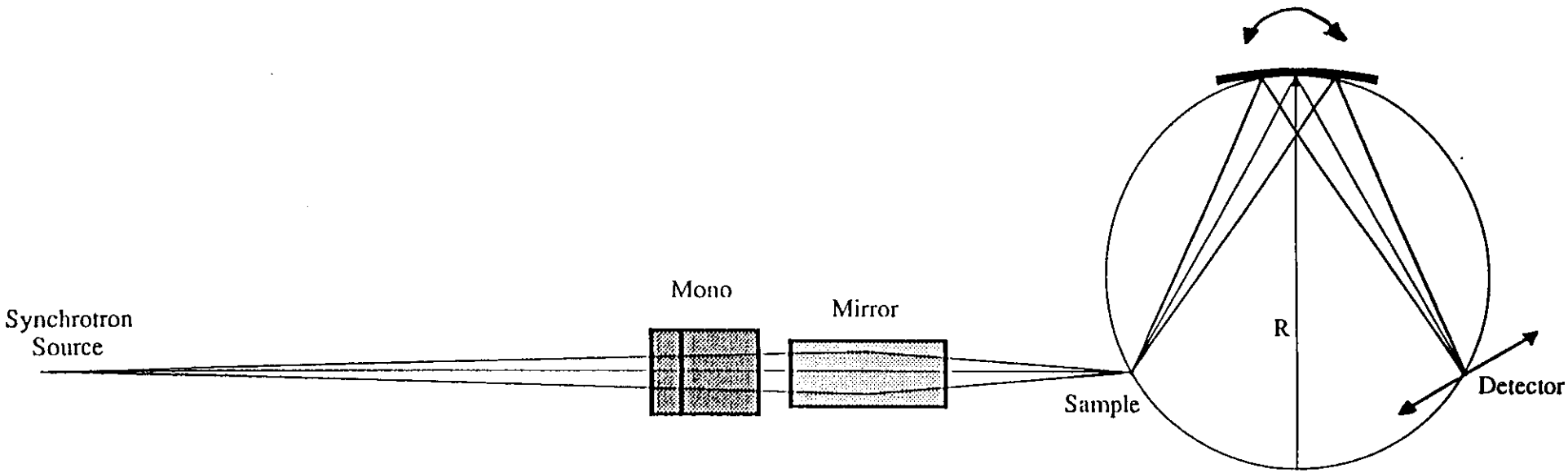


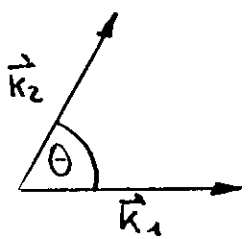


$$\left(\frac{\Delta E}{E}\right)_{tot} = 10^{-4} - 10^{-5}$$

# 1m Spherical Crystal Rowland Spectrometer

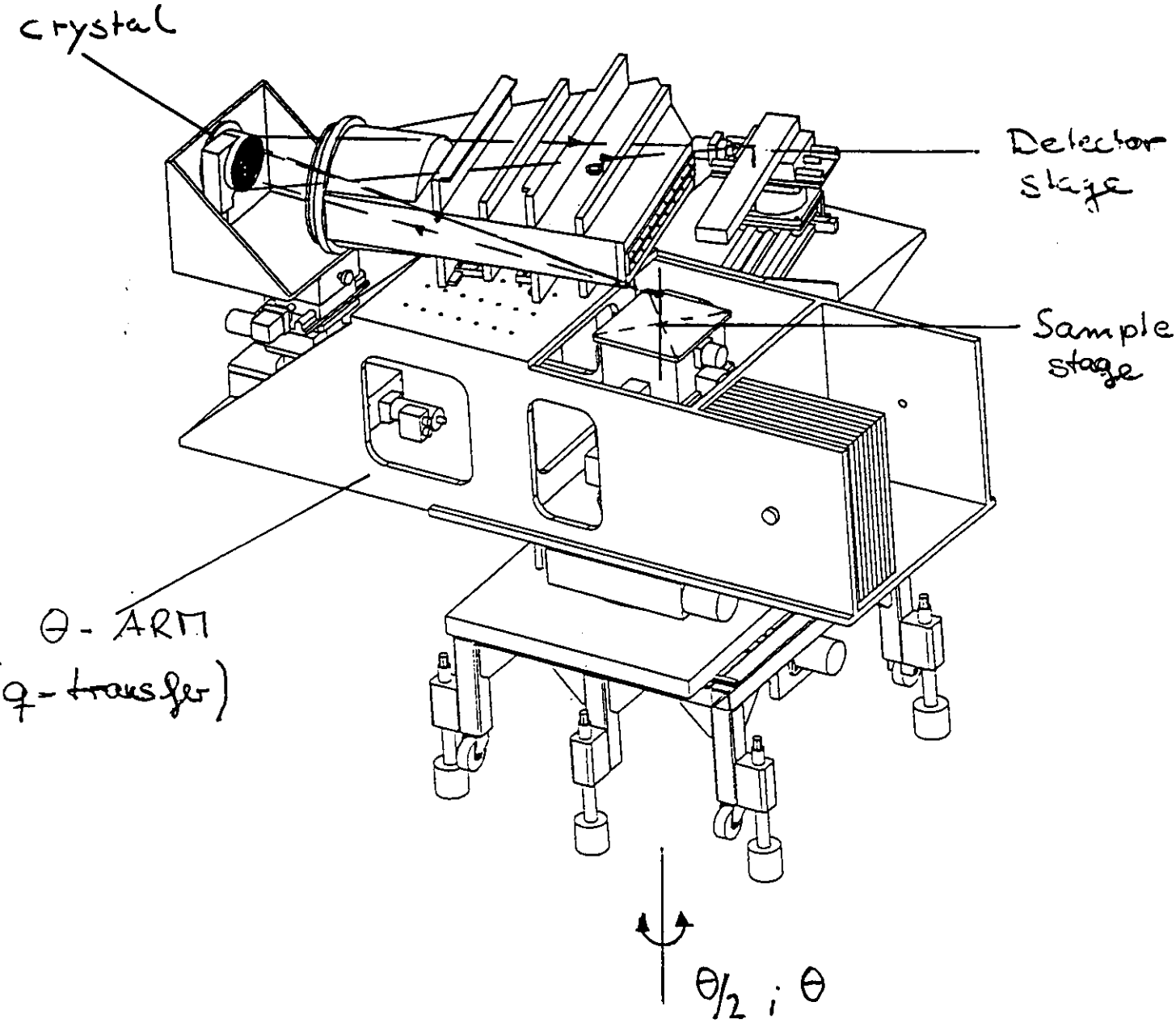

# Experimental Setup ID16/BL21 at the ESRF

Incident x-rays, vertical scattering plane

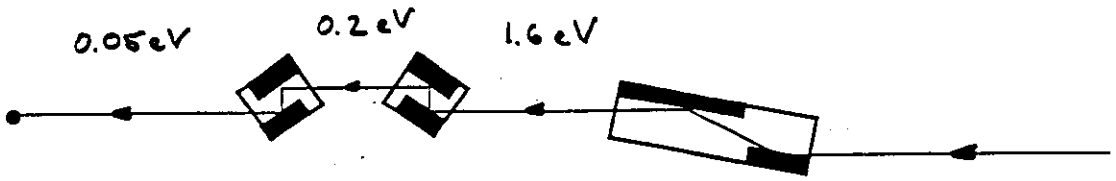


sample | Si(444), α,-α | Si (111), α=0 | undulator

Scattered x-rays, horizontal scattering plane

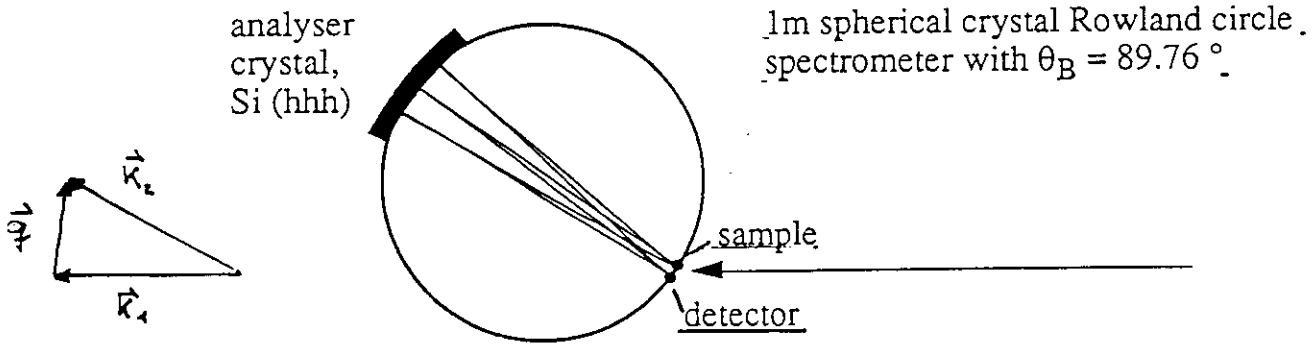


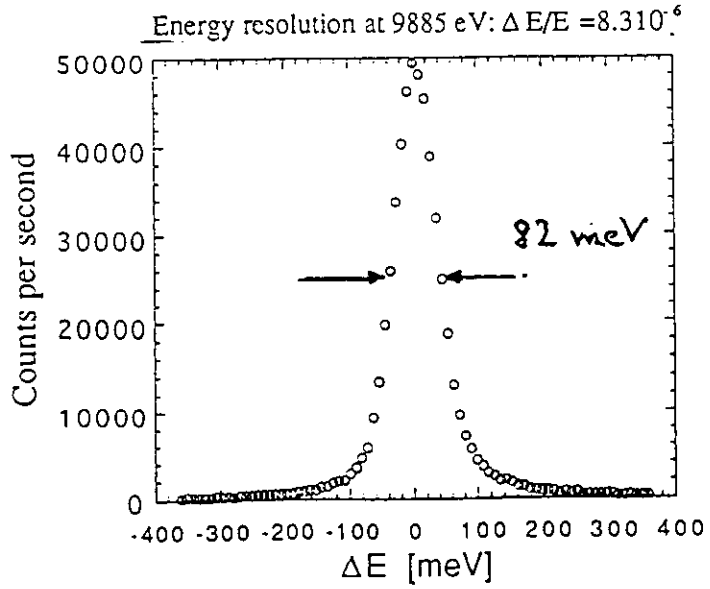

# Resonant Inelastic X-ray Scattering

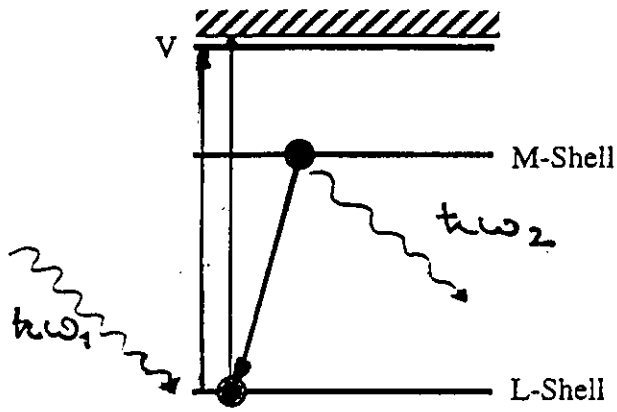


$$\frac{d^2\sigma}{d\Omega\, d\hbar\omega_2} = r_0^2 \frac{\omega_2}{\omega_1} \sum_{q,q'} \sum_{F} \left| \frac{1}{m_e} \sum_{N} \frac{\langle F | D_{q'}^{(L)} | N \rangle \langle N | D_{q}^{(L)} | I \rangle}{E_I - E_N + \hbar\omega_1 + 0.5i\Gamma_N} \right|^2 \delta\left(E_F - E_I - \hbar\omega\right)$$

- Energy resolution of RIXS spectra limited by $\Gamma_F$
- Resonance condition, if $\hbar\omega_1 = E_N - E_I$
- Below threshold: $\hbar\omega_1 < E_N - E_I$
  Raman dispersion: $\hbar\omega_2 = \hbar\omega_1 - (E_F - E_I)$
- Above threshold: $\hbar\omega_1 > E_N - E_I$
  - $\hbar\omega_2$ = constant for excitations into continuum states
  - $\hbar\omega_2$ = dispersing with $\hbar\omega_1$ for excitations into a discrete state

Energy Conservation: $E_F - E_I = \hbar\omega_1 - \hbar\omega_2$

$\hbar\omega_1 < E_{1s}$:

$$\hbar\omega_1 - \hbar\omega_2 = E_{2p} + \varepsilon$$

$$\Rightarrow \quad \hbar\omega_2 = \hbar\omega_1 - E_{2p} - \varepsilon$$

$\hbar\omega_1 > E_{1s}$: (i) excitation into continuum states

$$\hbar\omega_1 - \hbar\omega_2 = E_{2p} + \varepsilon$$

$$\hbar\omega_1 = E_{1s} + \varepsilon$$

$$\Rightarrow \quad \hbar\omega_2 = E_{1s} - E_{2p}$$

(ii) excitation into a discrete state $E^*$ below the onset of the continuum states

$$\hbar\omega_1 - \hbar\omega_2 = E_{2p} - E^*$$

$$\hbar\omega_2 = \hbar\omega_1 - E_{2p} + E^*$$

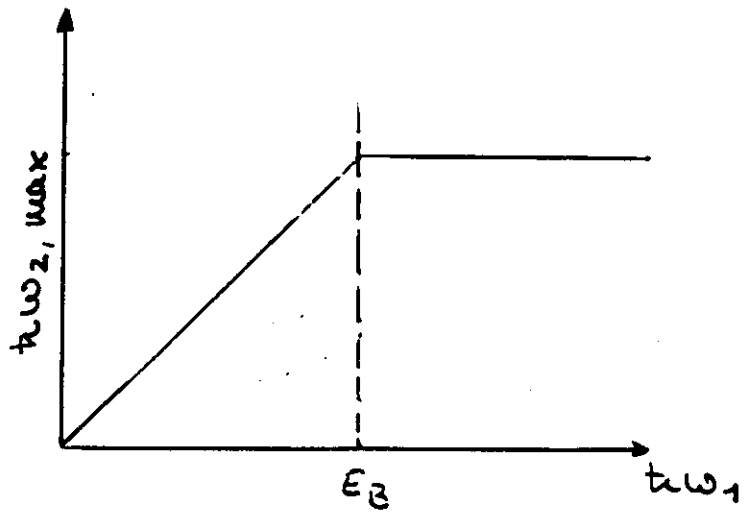
ħω2, max
E_B
ħω1

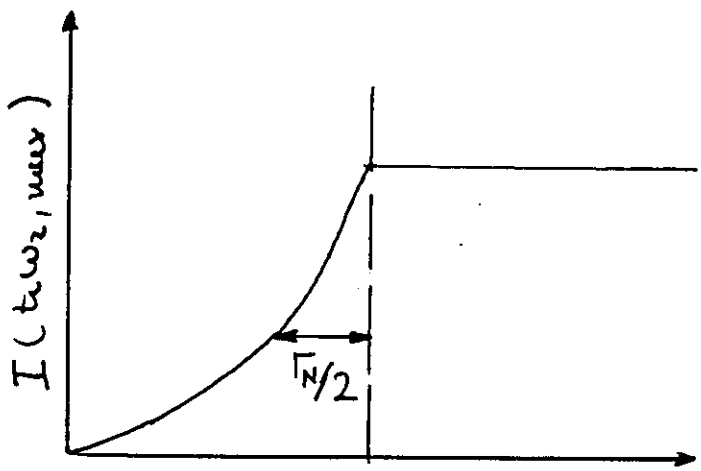
I(ħω2, max)
Γ_N/2

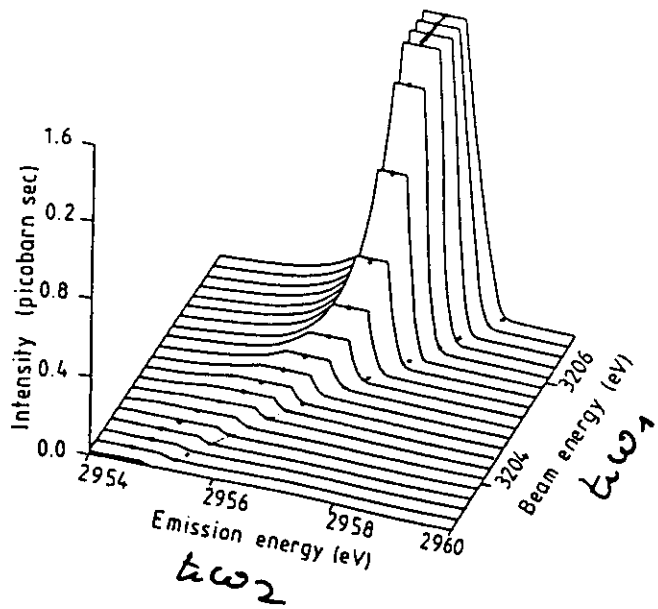
1.6
0.2
0.8
0.4
0.0
Intensity (picobarn sec)
2954
2956
2958
2960
Emission energy (eV)
ħω2
3206
3204
Beam energy (eV)
ħω1

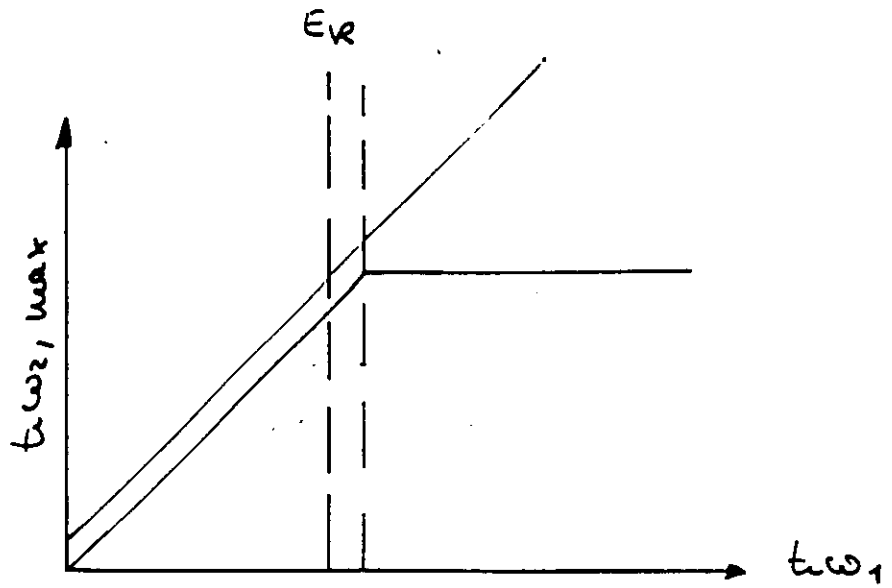
$E_R$
$\hbar\omega_{2,max}$
$\hbar\omega_1$

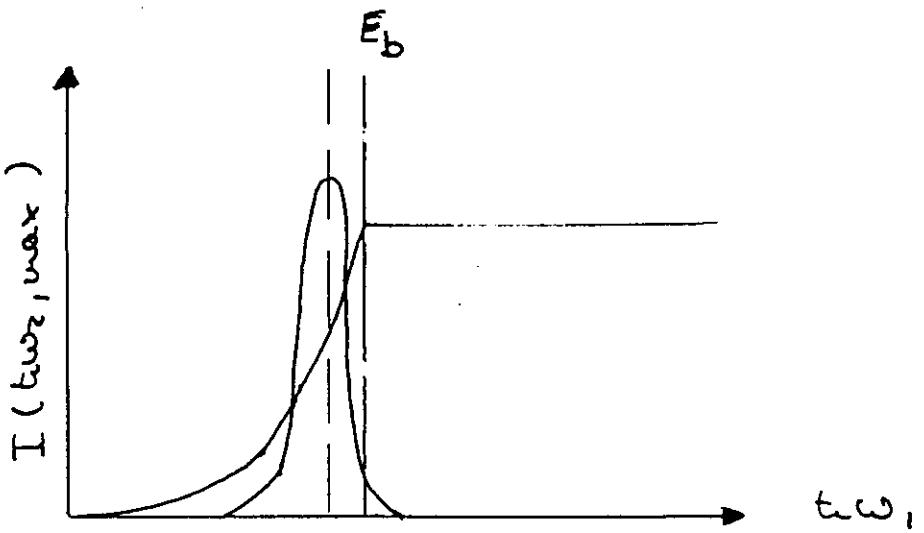
$E_b$
$I(\hbar\omega_{2,max})$
$\hbar\omega_1$

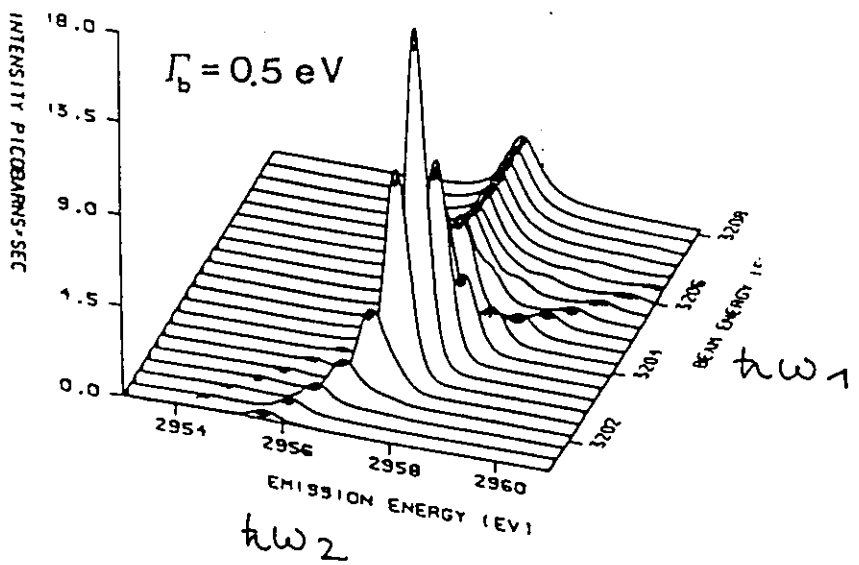
$\Gamma_b = 0.5$ eV
INTENSITY PICOBARNS/SEC
18.0
13.5
9.0
4.5
0.0
2954
2956
2958
2960
EMISSION ENERGY (EV)
$\hbar\omega_2$
$\hbar\omega_1$

# RIXS at the $L_3$-edge of Gd in $Gd_3Ga_5O_{12}$

- Motivation:

Assess the multipolar nature of the XMCD signal at the L-edges of Rare Earths materials.

G. Schütz et al.; Z. Phys. B 73, 67 (1988)

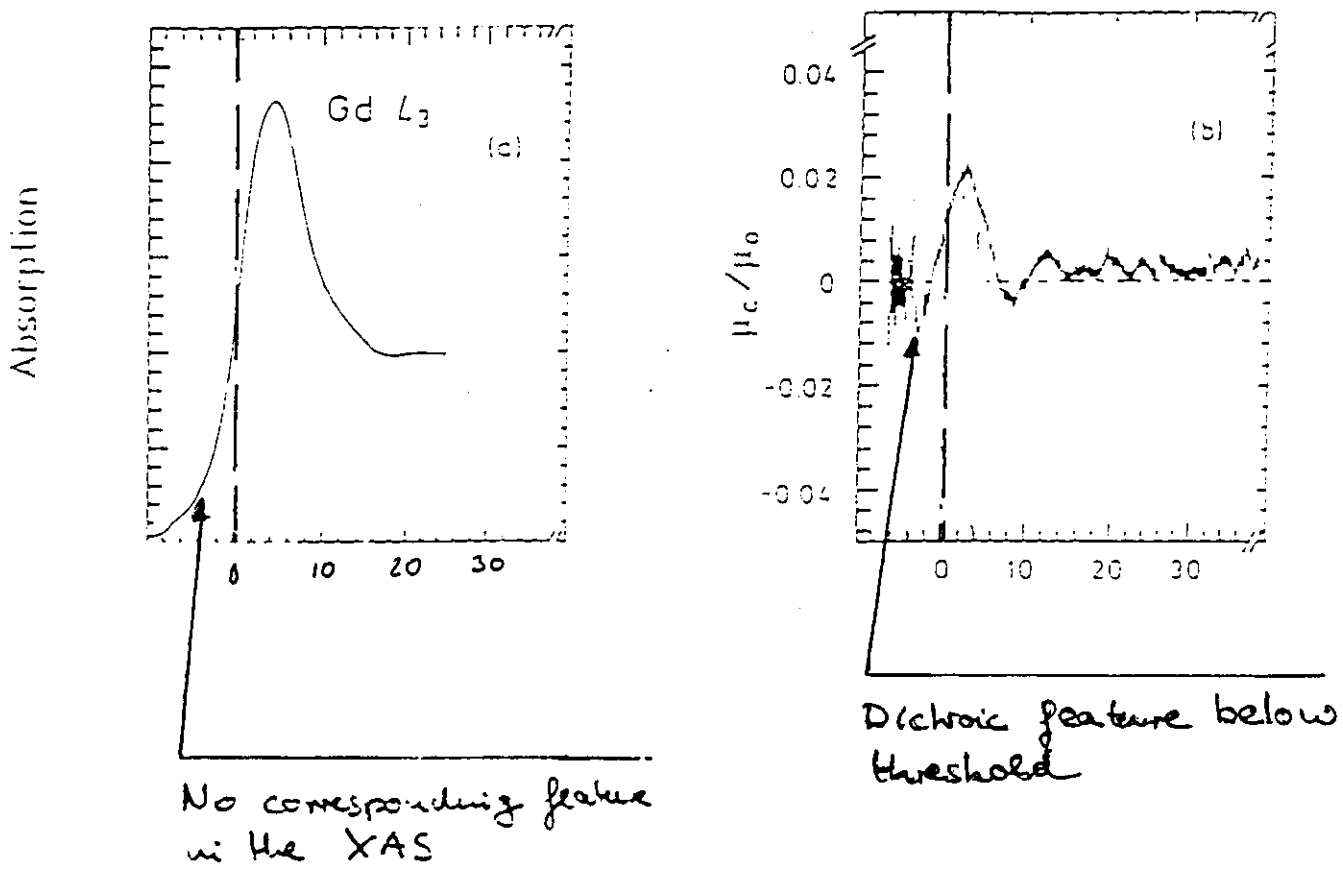


- D. Gibbs et al.; Phys. Rev. Lett. 61, 1241 (1988)
- P. Carra et al.; Phys. Rev. Lett. 66, 2495 (1991)
- J.C. Lang et al.; Phys. Rev. Lett. 74, 4935 (1995)
- C. Georgetti et al.; Phys. Rev. Lett. 75, 3186 (1995)

M. Krisch, C.C. Kao, F. Sette, W. Caliebe, K. Hämälainen, and J. Hastings; Phys. Rev. Lett. 74, 4931 (1995)

# X-Ray Magnetic Circular Dichroism

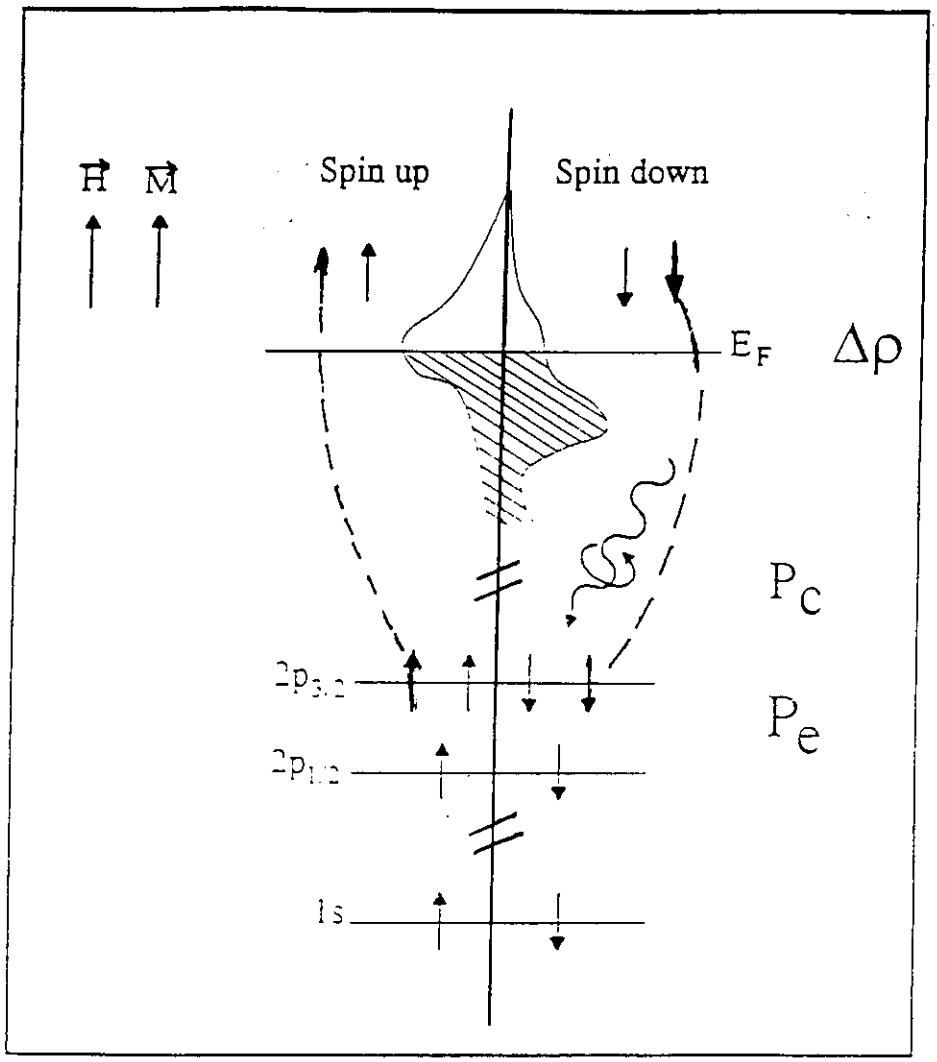


- Creation of a spin-polarized core-hole
  (magnetically aligned system + circular polarized x-rays)
- Spin-Polarization of the final state
  (difference between spin-up and spin-down empty states)

$$\frac{\Delta\sigma}{\sigma} = P_c \cdot P_e \frac{\Delta\rho}{\rho}$$

- element + symmetry selective information on the polarization of electronic states above the Fermi level

# RIXS at the $L_3$-edge of Gd in $Gd_3Ga_5O_{12}$

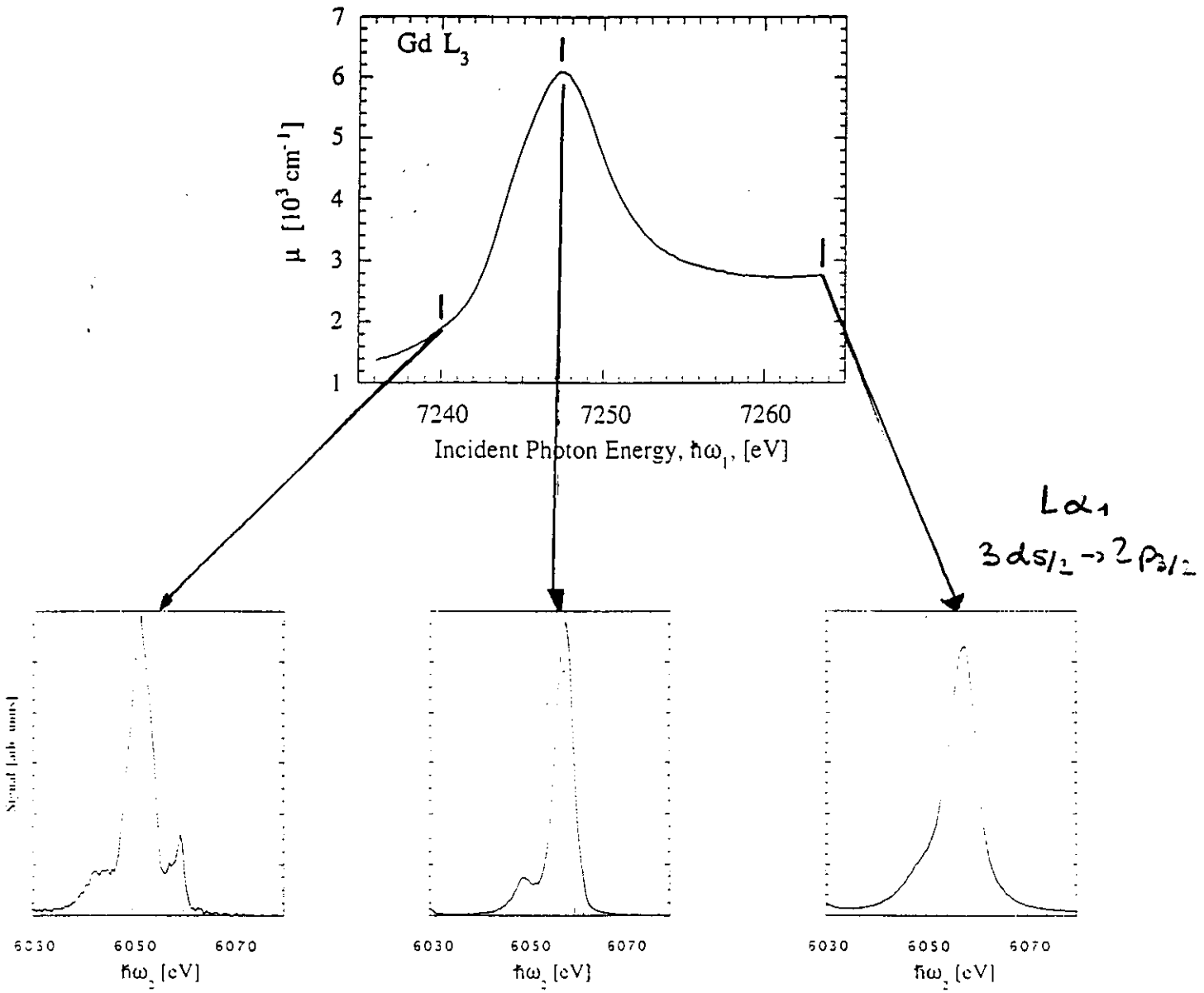


- $I(\hbar\omega_2)$ for fixed $\hbar\omega_1$ around the $L_3$ absorption edge

$$\left|4f^7 5d^0\right\rangle \text{->} \left|\underline{2p^5} 4f^n 5d^{n'}(\varepsilon)\right\rangle \text{->} \left|\underline{3d^9} 4f^n 5d^{n'}(\varepsilon)\right\rangle$$

**X21 at NSLS:** M.H. Krisch, C.C. Kao, F. Sette, W. Caliebe, K. Hämälainen, and J. B. Hastings; Phys. Rev. Lett. 74, 4931 (1995).

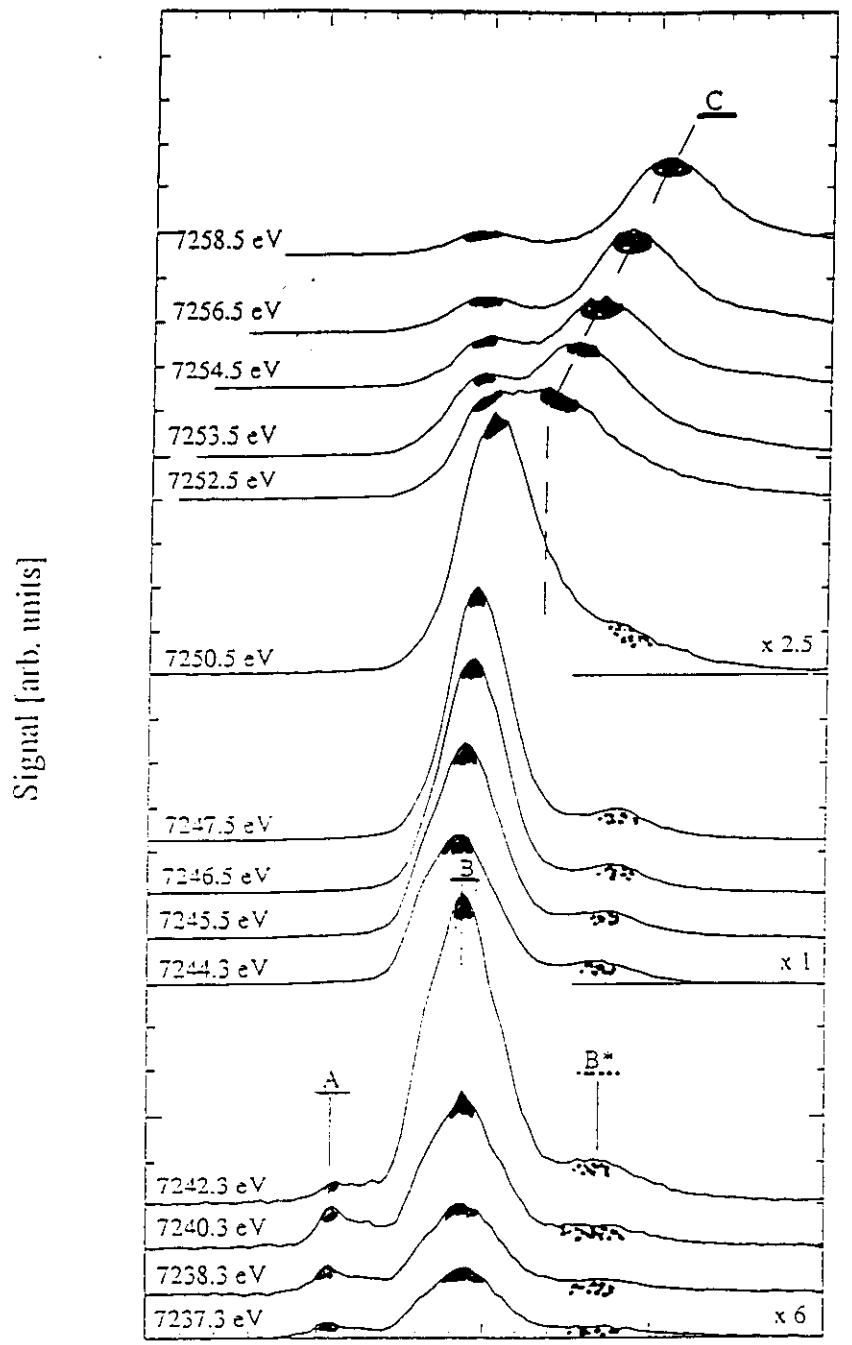


- $\left|4f^7 5d^0\right\rangle \rightarrow \left|2p^5 \underline{4f^8} 5d^0\right\rangle \rightarrow \left|3d^9 \underline{4f^8} 5d^0\right\rangle$
- $\left|4f^7 5d^0\right\rangle \rightarrow \left|2p^5 4f^7 \underline{5d^1}\right\rangle \rightarrow \left|3d^9 4f^7 \underline{5d^1}\right\rangle$
- $\left|4f^7 5d^0\right\rangle \rightarrow \left|2p^5 4f^7 5d^0 \underline{\varepsilon}\right\rangle \rightarrow \left|3d^9 4f^7 5d^0 \underline{\varepsilon}\right\rangle$

- $|F\rangle_A$ has the lowest final state energy, since an extra electron in the localized 4f orbitals has a larger Coulomb interaction with the 3d core hole, making a more tightly bound final state in comparison to an electron promoted either to the 5d orbitals or to the continuum.

- Calculation of the E2-part of the RIXS spectrum for Gd:
  M. van Veenendaal, Phys. Rev. **B 54**, 16010 (1996).

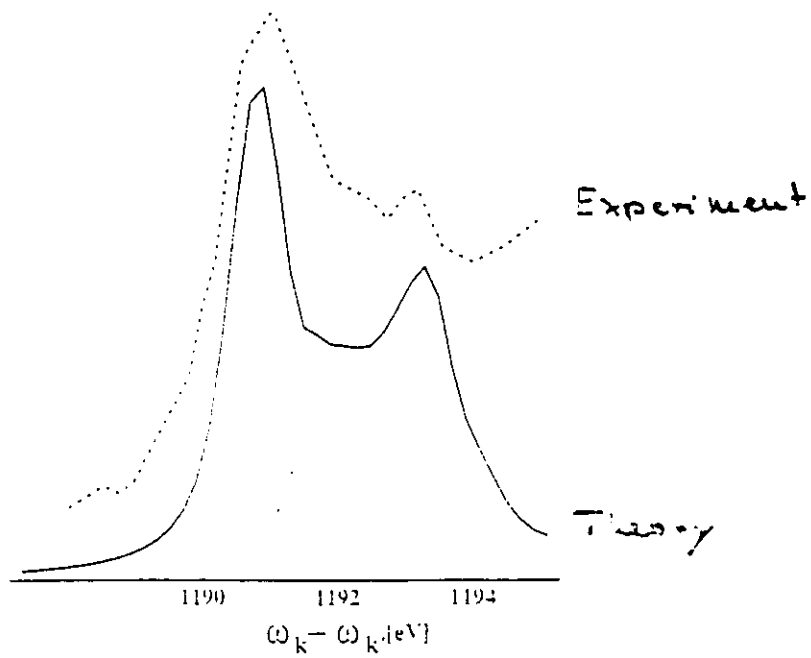


Direct comparison with x-ray absorption spectrum:

Constant Final State Scan: $E_F - E_I = \hbar\omega_1 - \hbar\omega_2 = \text{constant}$

- $I(\hbar\omega_1 - \hbar\omega_2 = \text{constant}, \hbar\omega_1)$

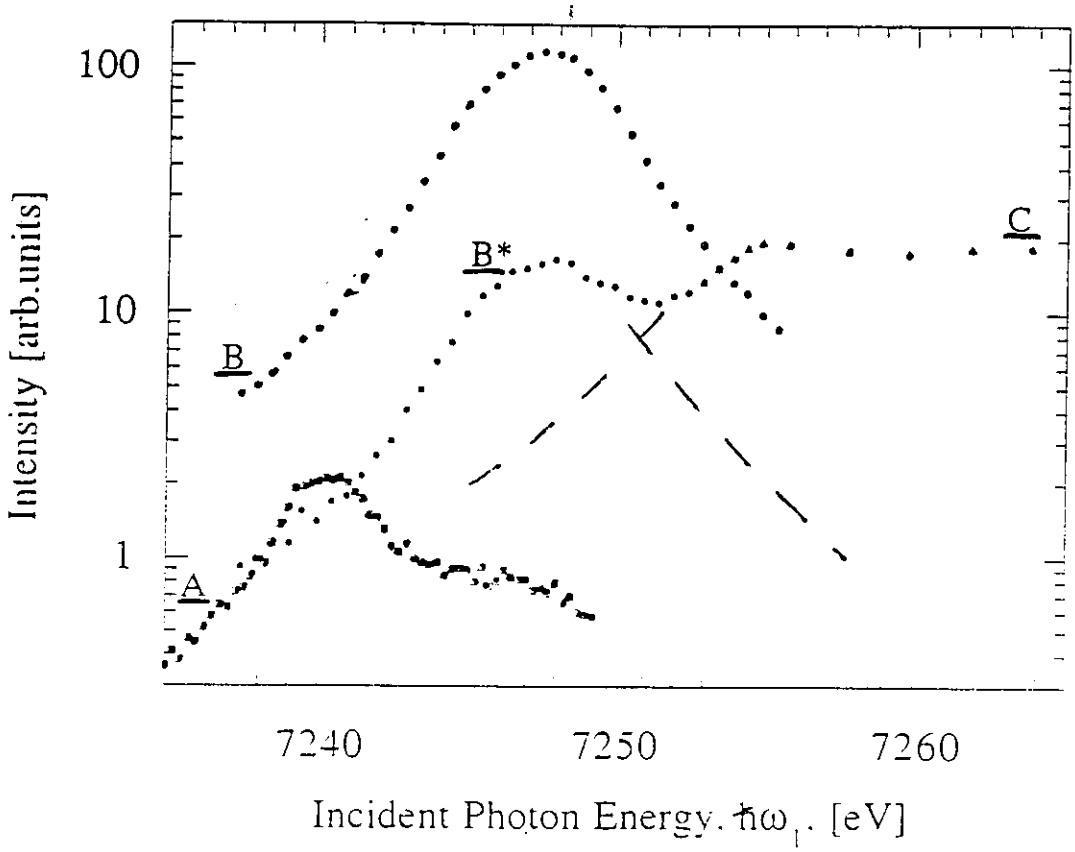


- Separation of different excitation channels contributing to the same absorption edge.

- Existence, strength and location of the quadrupolar excitation channel at the Gd $L_3$-edge:

| E2/E1 = 0.018 | $\Delta E_{1,2}$ = 7.5 eV |
|---|---|

Condition:

| Final state core-hole lifetime < energy separation of the multiplet families |
|---|

# RIXS at the $L_3$-edge of Er in $Er_2O_3$

**ID26 (ESRF):** C. Dallera, M. Krisch, C. Gauthier, A. Sole, A. Rogalev, J. Goulon, F.Sette

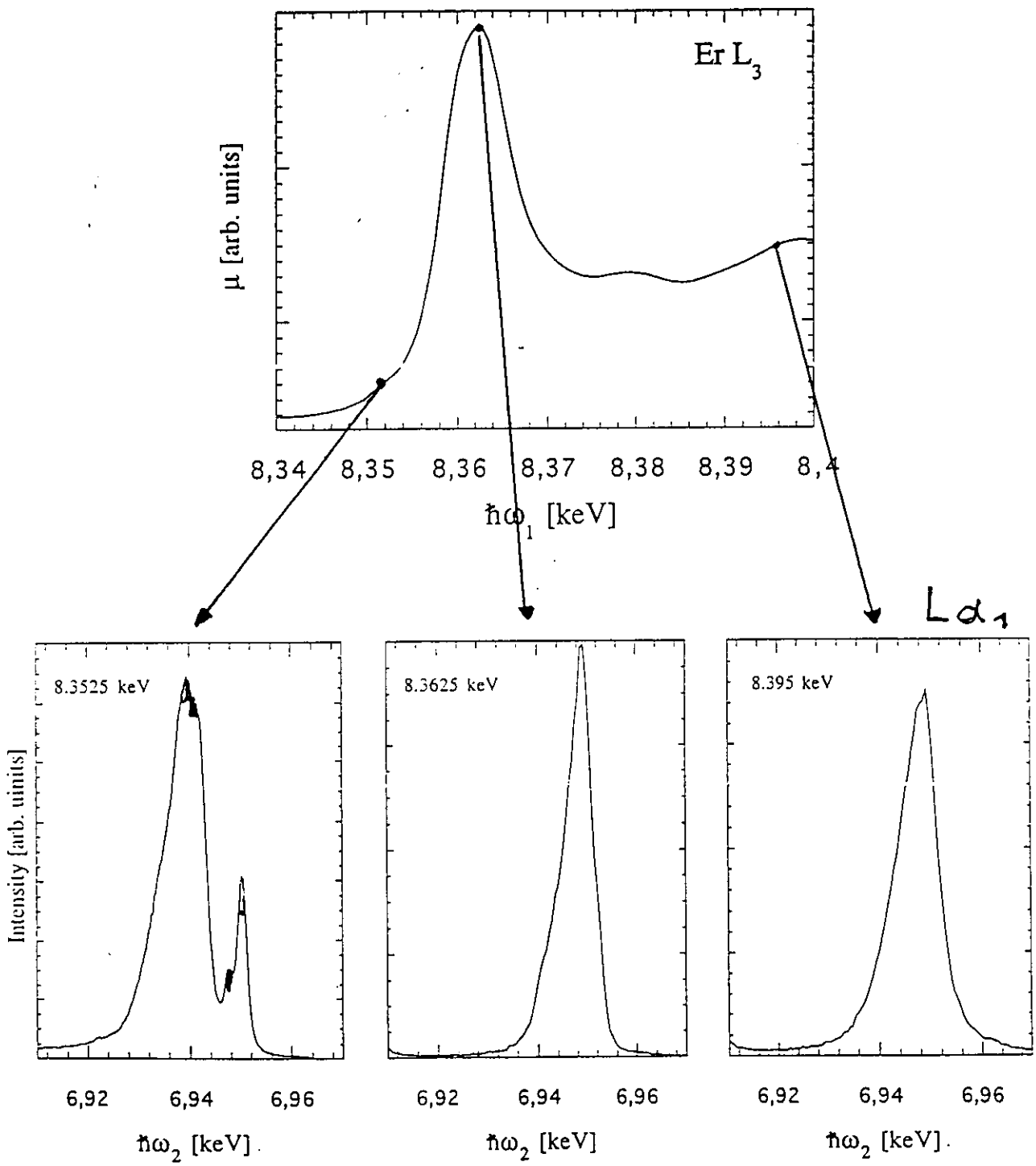


$$\left|4f^{11}5d^{0}\right\rangle -> \left|\underline{2p^{5}}4f^{n}5d^{n'}(\varepsilon)\right\rangle -> \left|\underline{3d^{9}}4f^{n}5d^{n'}(\varepsilon)\right\rangle$$

# Constant Final State Scans

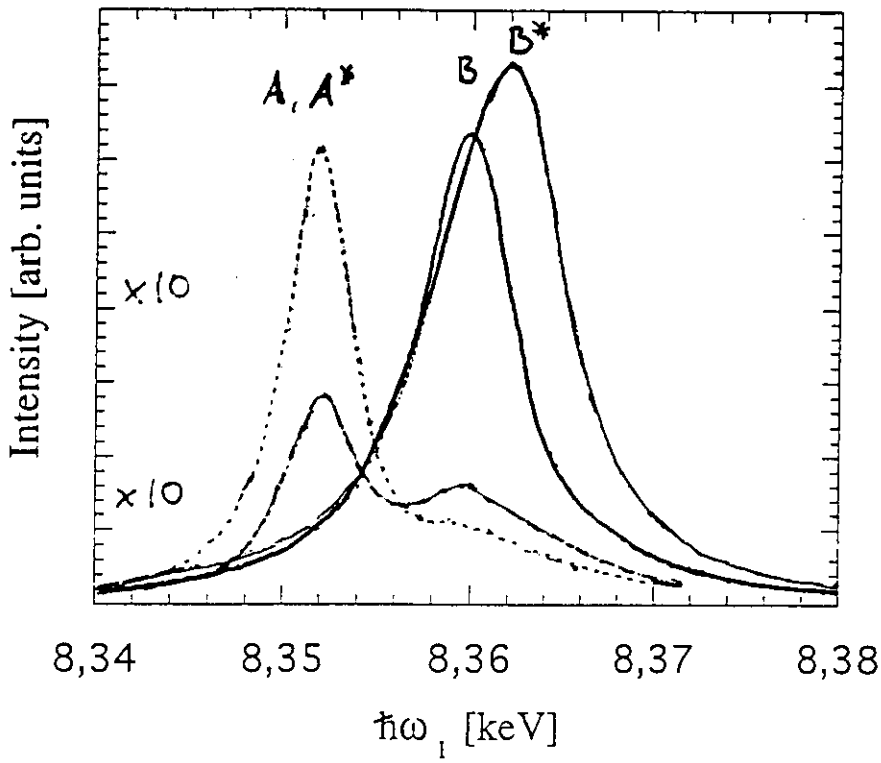


- B and B* belong to different intermediate states, and are due to the cubic crystal field splitting of the 5d states: $\Delta E = 2.3$ eV
- A and A* belong to the same intermediate state, and are due to the final state multiplet splitting.

# Identification of E2 Excitation Channels at the $L_3$ Edge of $RE_2Fe_{14}B$

• F. Bartolomé, J.M. Tonnerre, L. Sève, and D. Raoux (CNRS Grenoble)
J. Chaboy and L.M. Garcia (Zaragoza)
M. Krisch (ESRF), C.C. Kao (NSLS)

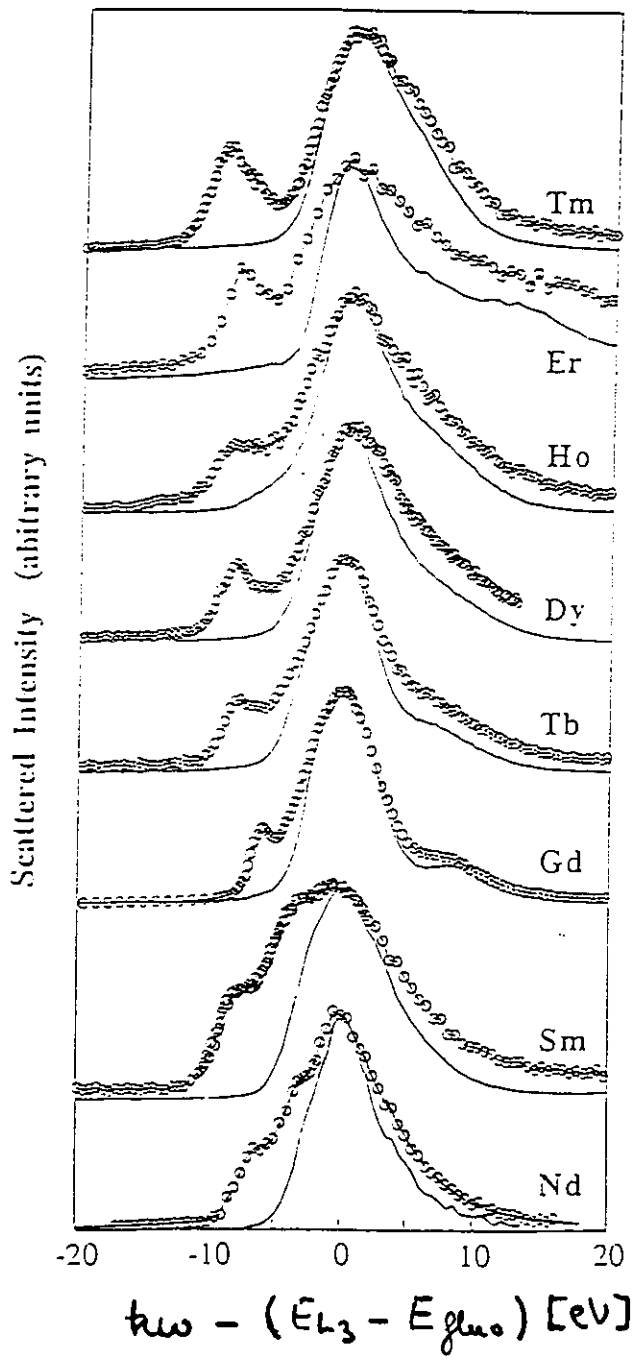

# Comparison XMCD - RIXS Constant Final State Spectra

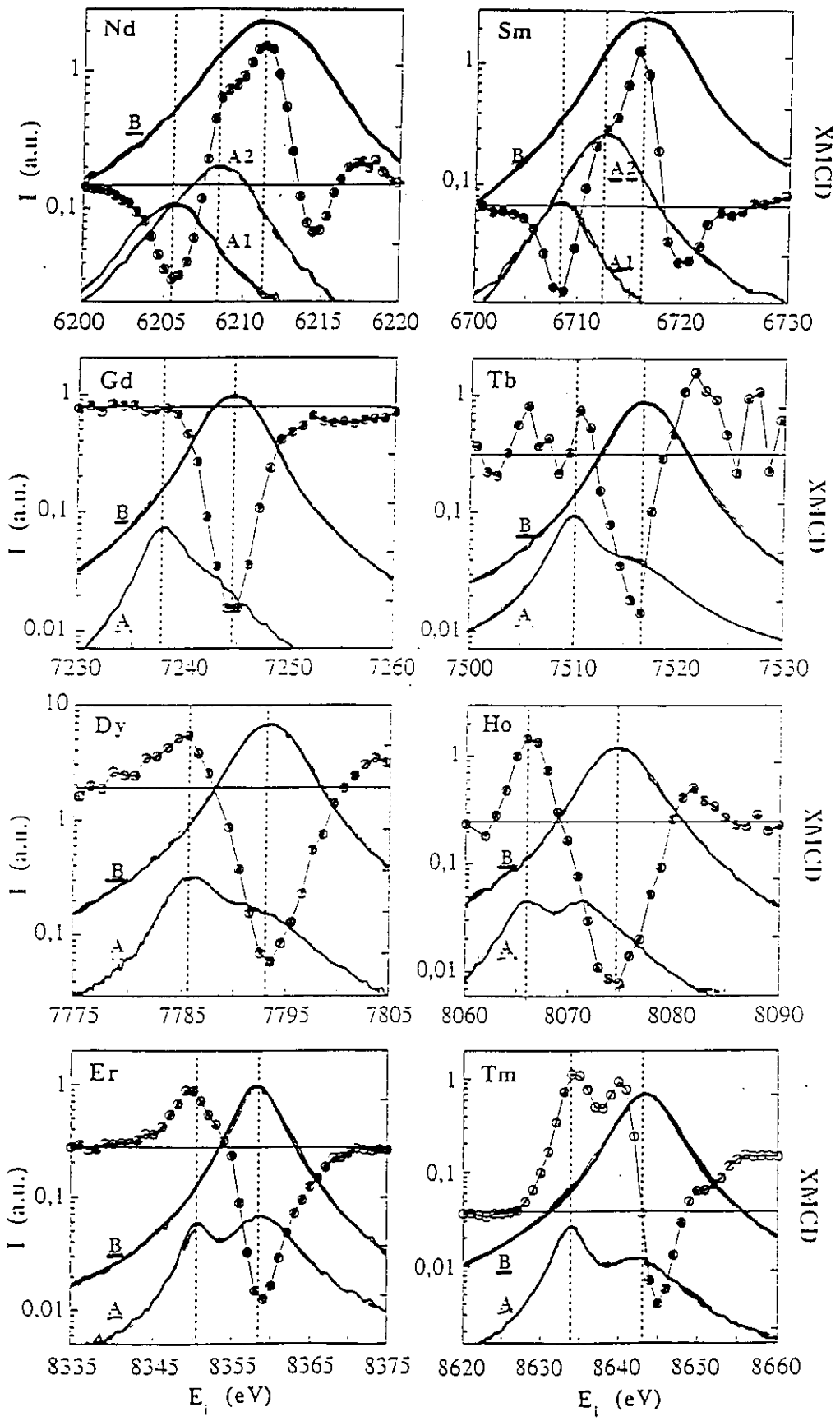

• Comparison XMCD - RIXS Constant Final State Spectra

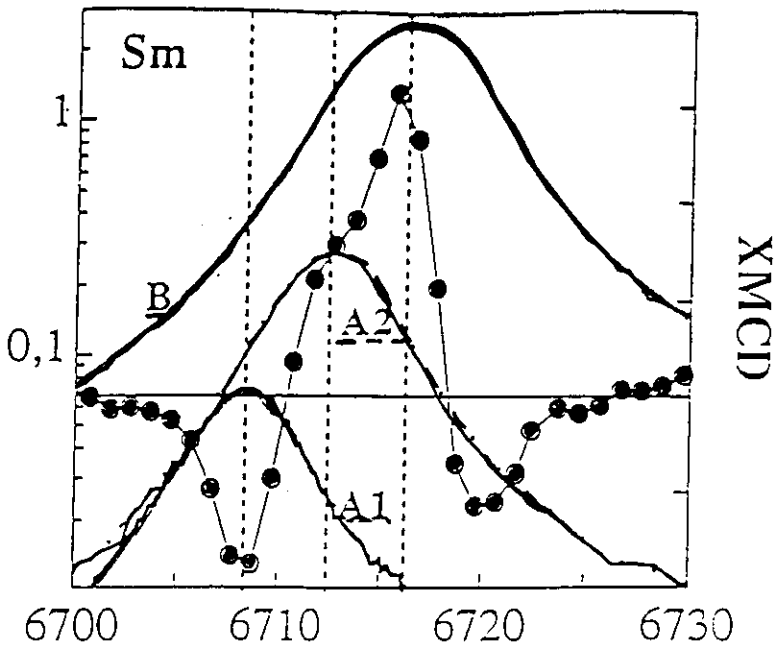


• Energy Difference $E_{E2}$ - $E_{WL}$

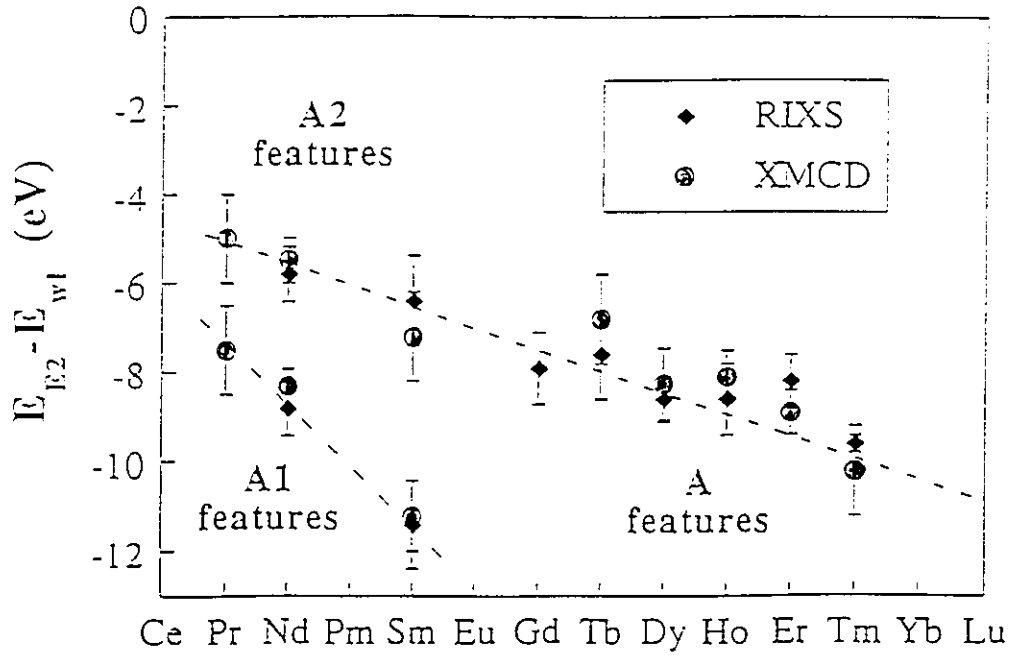

# RIXS at the K-edge of Fe in $Gd_3Fe_5O_{12}$

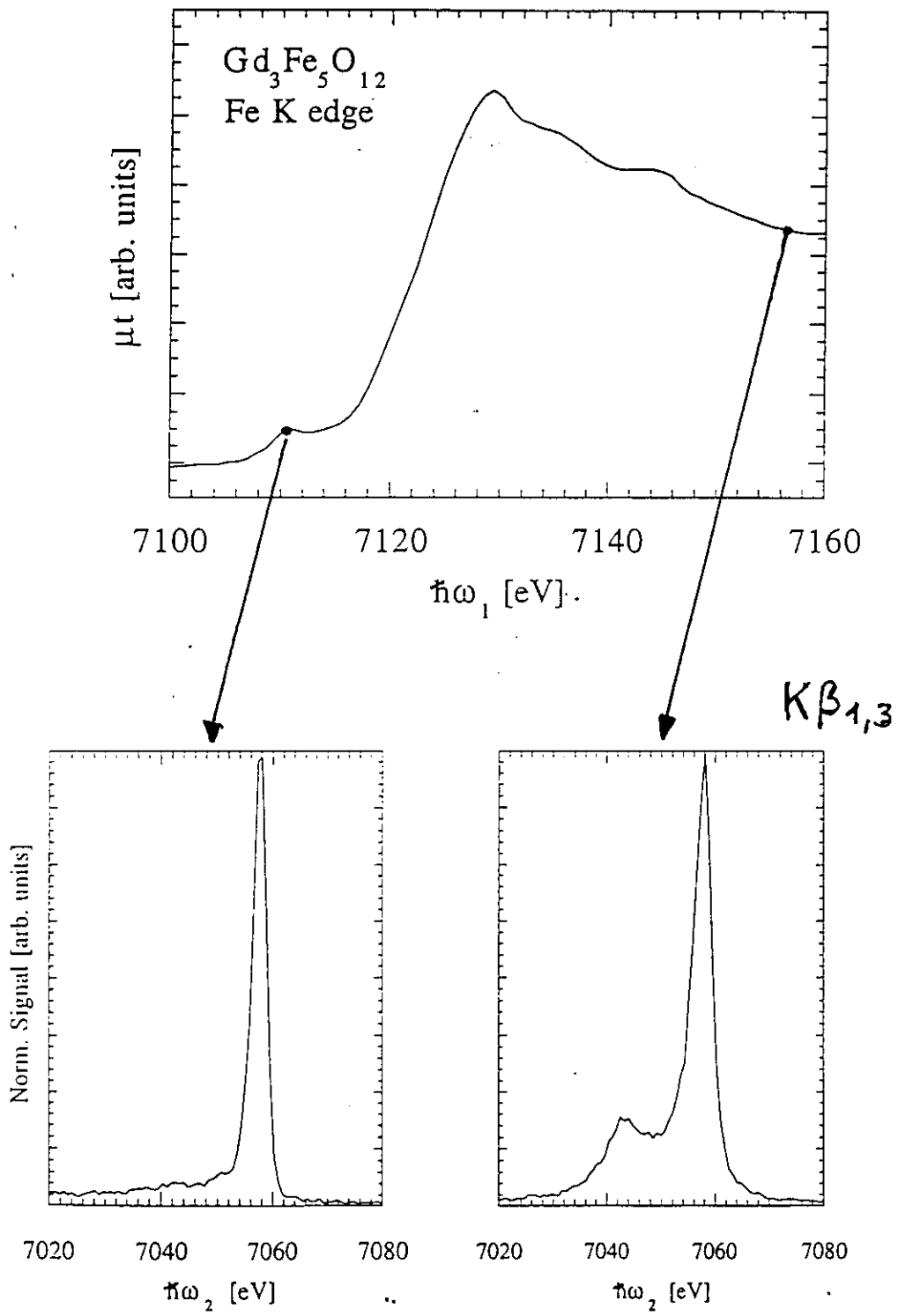


$$\left|3d^5\right\rangle \text{->} \left|\underline{1s^1}3d^n(\varepsilon)\right\rangle \text{->} \left|\underline{3p^5}3d^n(\varepsilon)\right\rangle$$

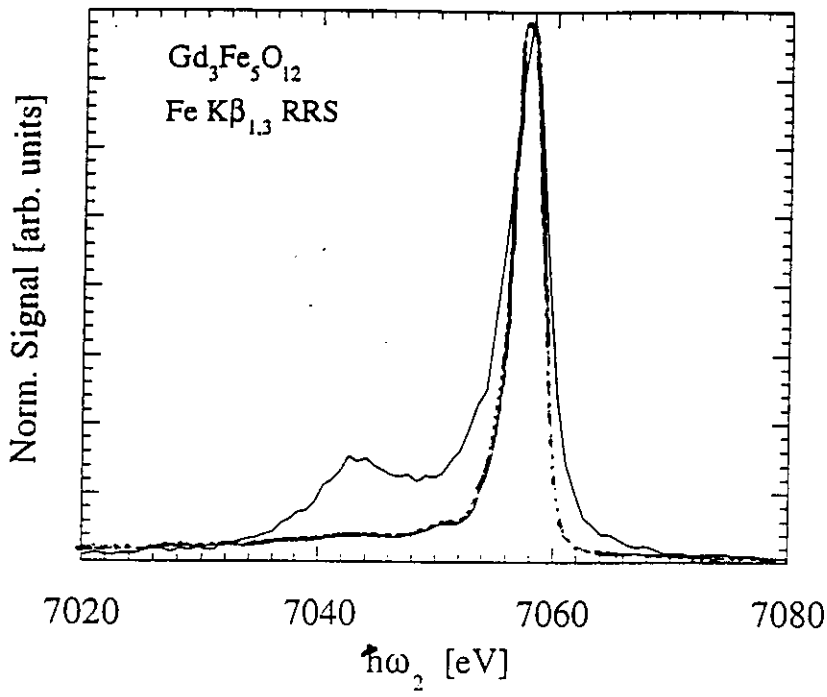


above threshold: $\left|3d^5\right\rangle \rightarrow \left|1s^1 3d^5 \varepsilon\right\rangle \rightarrow \left|3p^5 3d^5 \varepsilon\right\rangle$

at 1s -> 3d resonance: $\left|3d^5\right\rangle \rightarrow \left|1s^1 3d^6\right\rangle \rightarrow \left|3p^5 3d^6\right\rangle$

Above threshold final states with two different spin orientations between 3p- and 3d-shell possible.

$\left|3p_{\uparrow}^5 3d_{\uparrow}^5 \varepsilon_{\downarrow}\right\rangle$ lower final state energy => higher $\hbar\omega_2$

$\left|3p_{\downarrow}^5 3d_{\uparrow}^5 \varepsilon_{\uparrow}\right\rangle$ higher final state energy => lower $\hbar\omega_2$

For the 1s -> 3d transition, there are only spin-down vacancies!

Satellites typical in the fluorescence of elements with an incomplete electronic shell in the ground state.

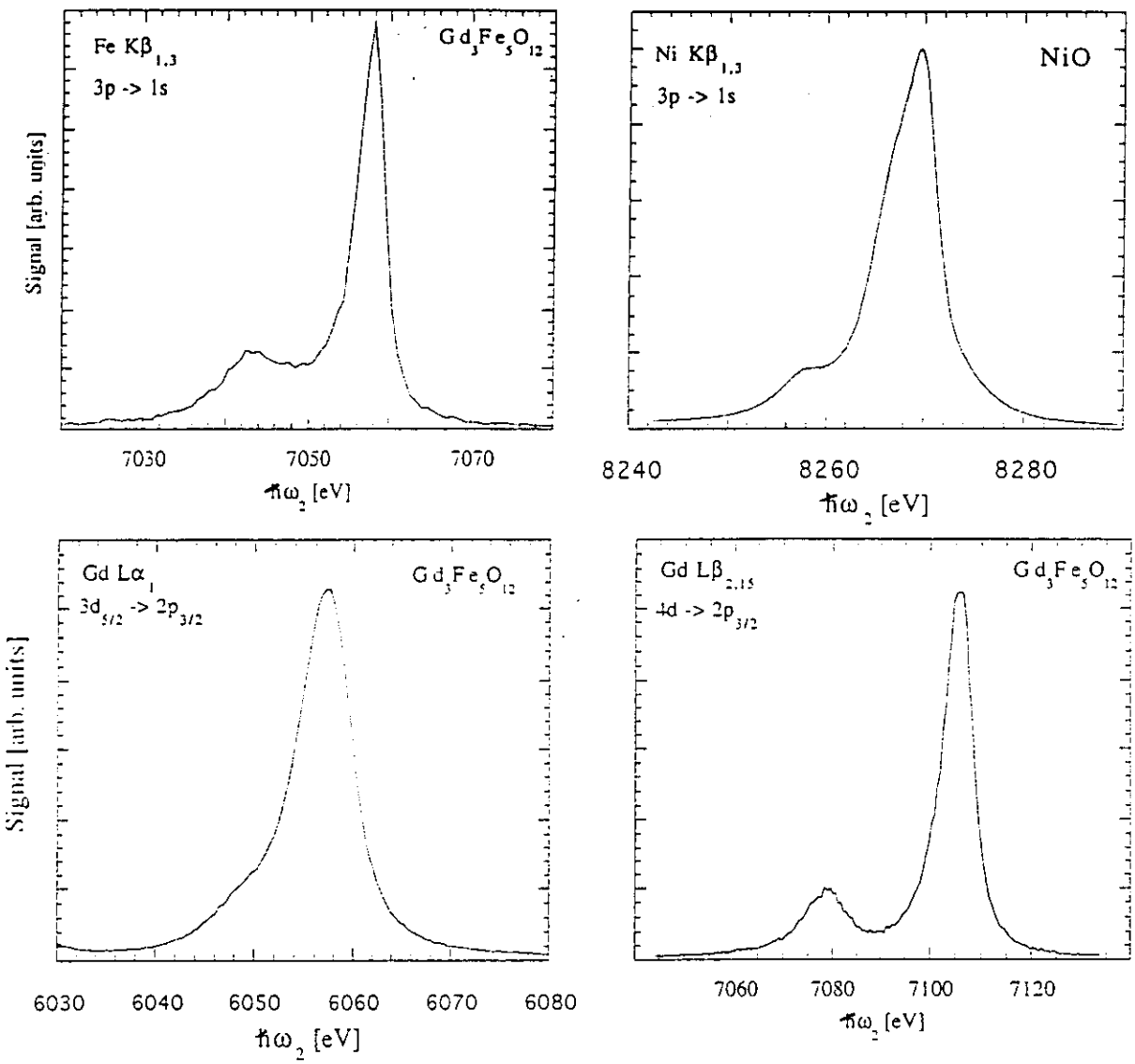


The fluorescence line shape reflects the interactions between the two incomplete electronic shells in the final state.

Main line: primarily spin-down character
Satellite: primarily spin-up character

# Local Spin-Selective X-ray Absorption

• The occurence of satellites in the fluorescence line is an intraatomic effect!

• No need for long range magnetic order and circular polarized x-rays to perform XMCD measurements!

XMCD

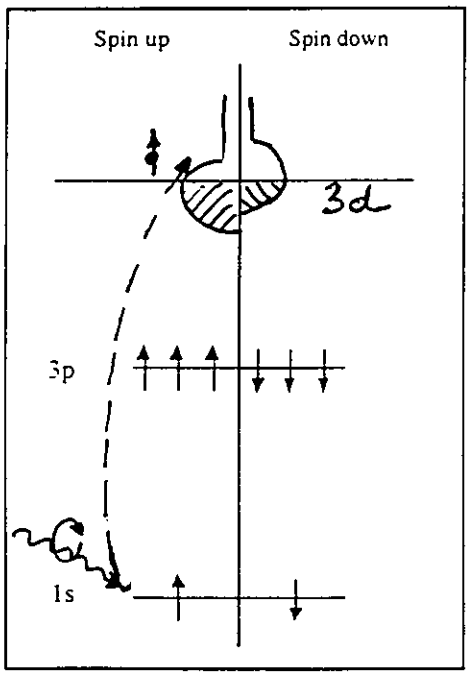


LSXAS

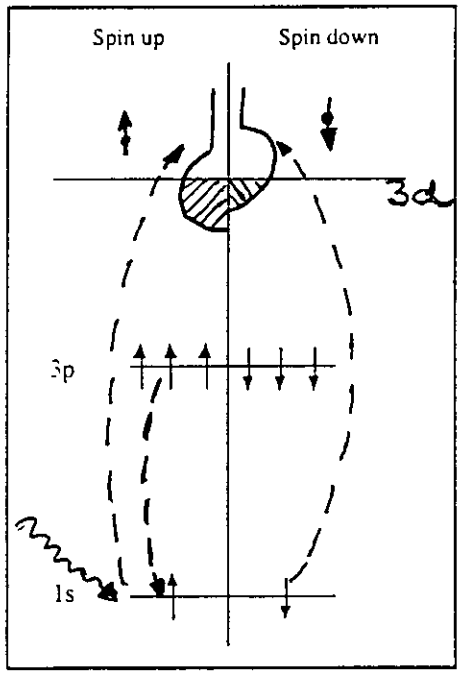


XMCD: $\mu_l(\hbar\omega_1) - \mu_r(\hbar\omega_1) = P_e\left[R^2_{\uparrow}(\hbar\omega_1)\rho_{\uparrow}(\hbar\omega_1)\right] - \left[R^2_{\downarrow}(\hbar\omega_1)\rho_{\downarrow}(\hbar\omega_1)\right]$

LSXAS: $\mu(\hbar\omega_1) - \mu(\hbar\omega_1) = \left[R^2_{\uparrow}(\hbar\omega_1)\rho_{\uparrow}(\hbar\omega_1)\right] - \left[R^2_{\downarrow}(\hbar\omega_1)\rho_{\downarrow}(\hbar\omega_1)\right]$

R: radial transition matrix element; $\rho_{\uparrow}$ , $\rho_{\downarrow}$ : spin-polarized empty density of states;
$P_e$: photoelectron polarization

# Ni Kβ - emission (3p -> 1s) in $CsNi[Cr(CN)_6]$

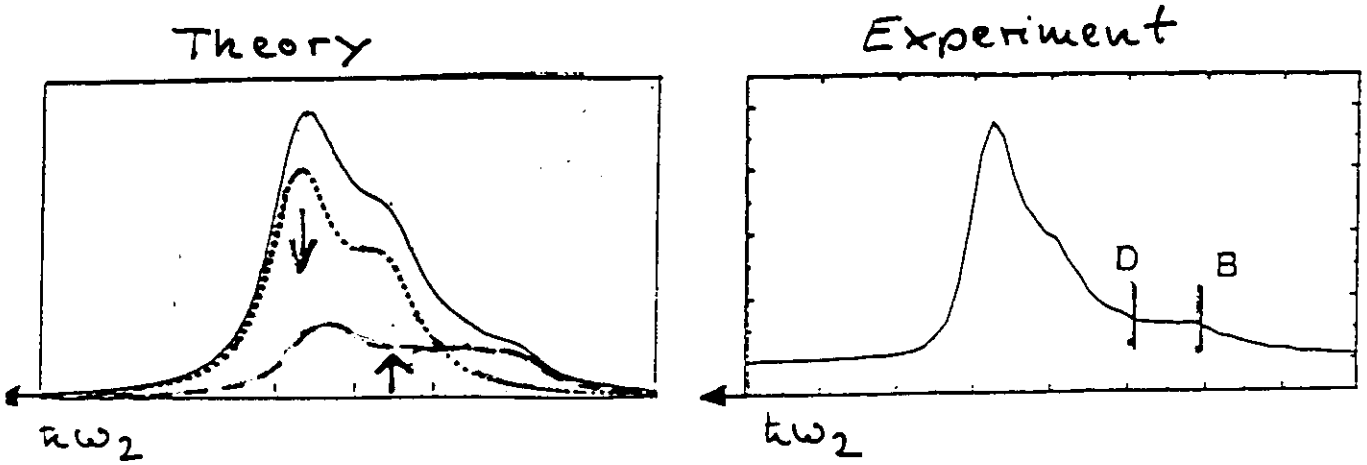


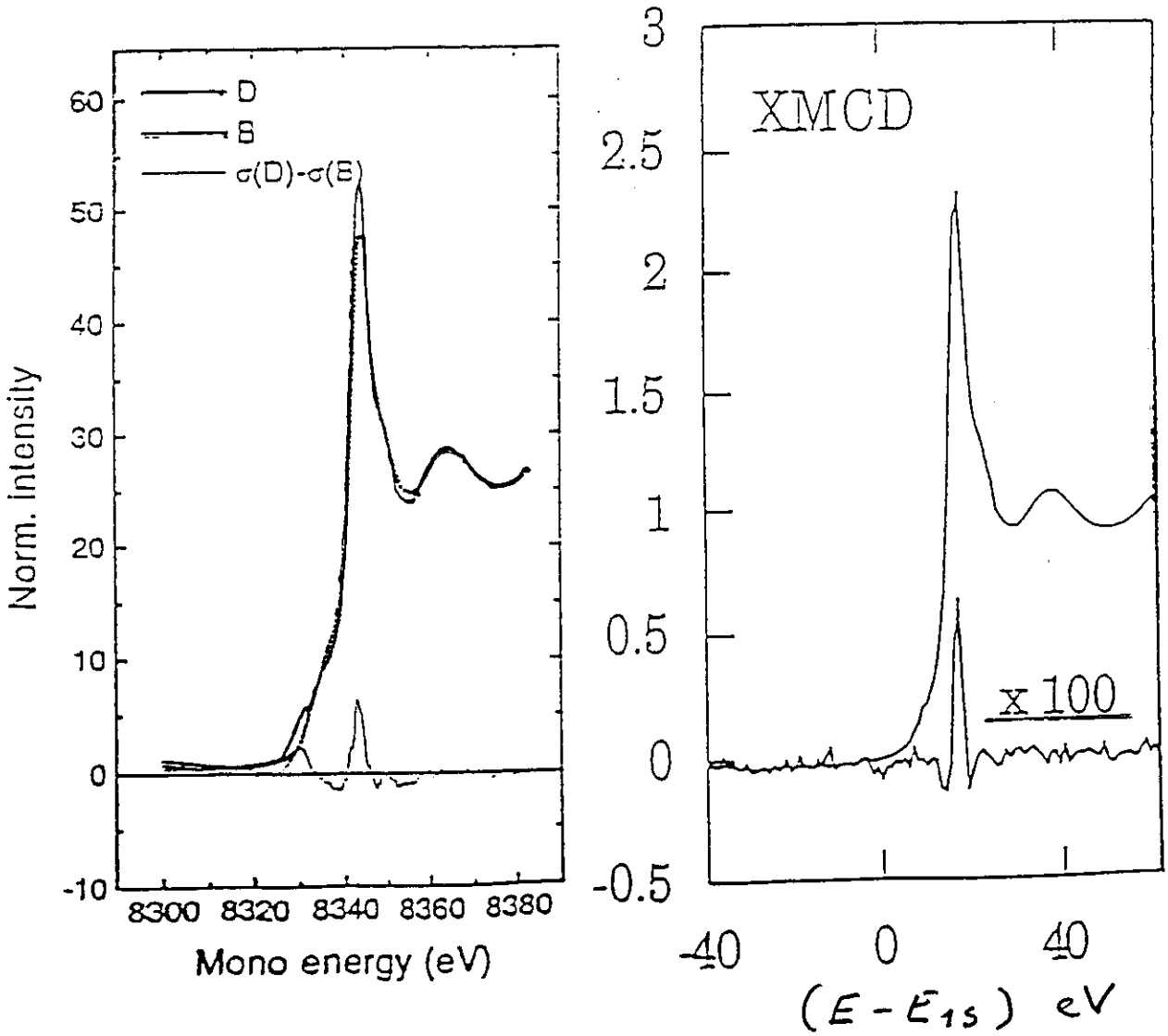

# Oxidation- and Spin-State Selectivity

(G. Peng et al.; J. Am. Chem. Soc. 116, 2914 (1994))

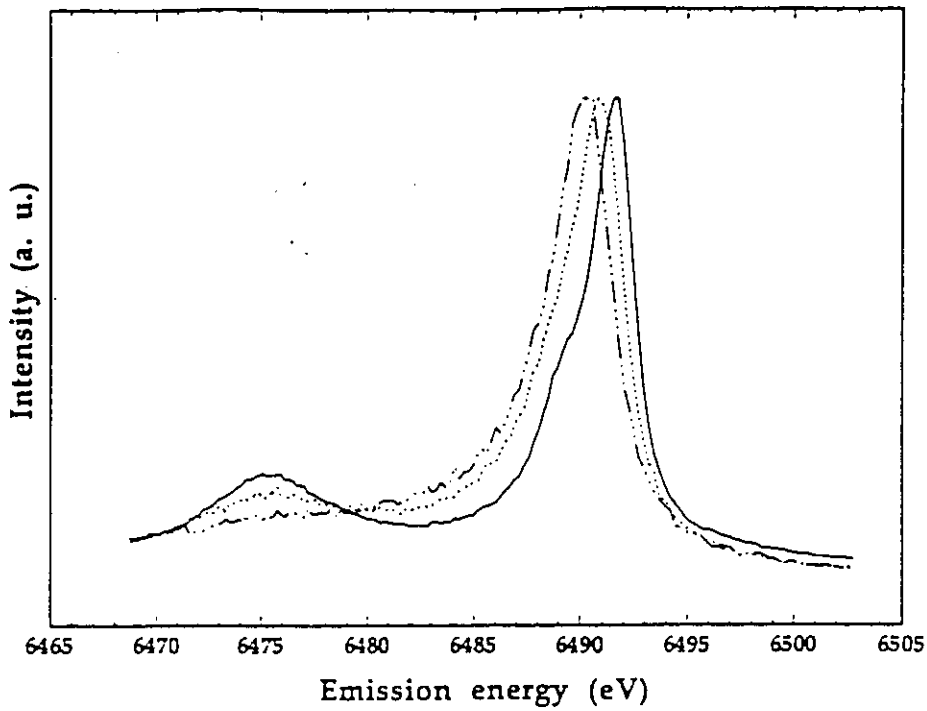


Figure 2. Oxidation-state effects on peak shapes and positions for Mn Kβ spectra: $Mn^{II}(OAc)_2$ (—); $Mn^{III}(OAc)_3$ (· · ·); $Mn^{IV}[HB(3,5\text{-}Me_2pz)_3]_2$-$(ClO_4)_2$ (· · – – ·).

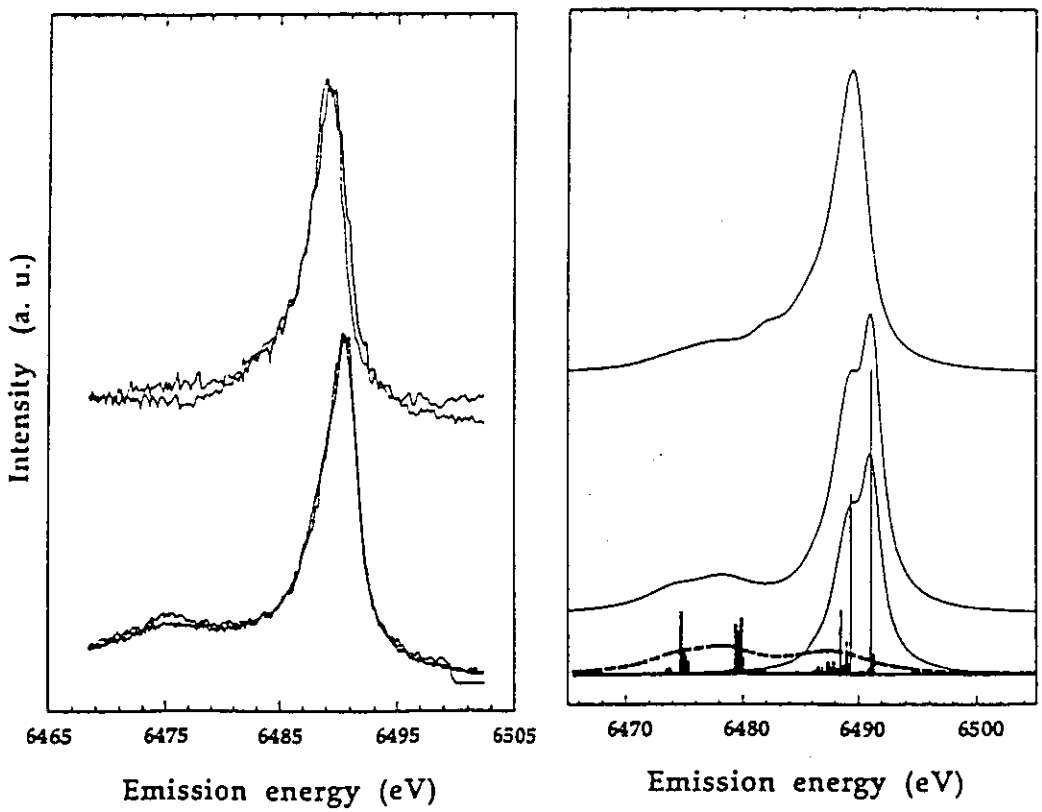


Figure 5. Left: Spectra of a representative series of Mn(III) compounds with different spin states. Key: top, low-spin $K_3Mn(CN)_6$ and $Mn[HB(3,5\text{-}Me_2pz)_3]_2$ $(ClO_4)$; bottom, high-spin $Mn(OAc)_3$, Mn(acen)Cl, Mn(P)Cl, and $Mn(phen)Cl_3$. Right: Calculated spectra of low spin (top) vs high-spin compounds (middle). Bottom spectra are the calculated spectra for $^7P_{4,3,2}$ (—) and $^5P_{3,2,1}$ (· · ·) final states, which give the middle summation spectrum. The calculated spectra are broadened with Lorentzian broadenings of 1.0 eV for the $K\beta_{1,3}$ structure and 2.0 eV for the $K\beta'$ as well as a Gaussian broadening of 0.5 eV.

# RIXS excited with circular polarized x-rays

- Creation of a spin-polarized $2p_{3/2}$ core-hole by excitation with circular polarized x-rays.
- Excitation well above threshold => no spin polarization in the intermediate state.
- Decay of an electron with the same spin orientation as the excited photoelectron.

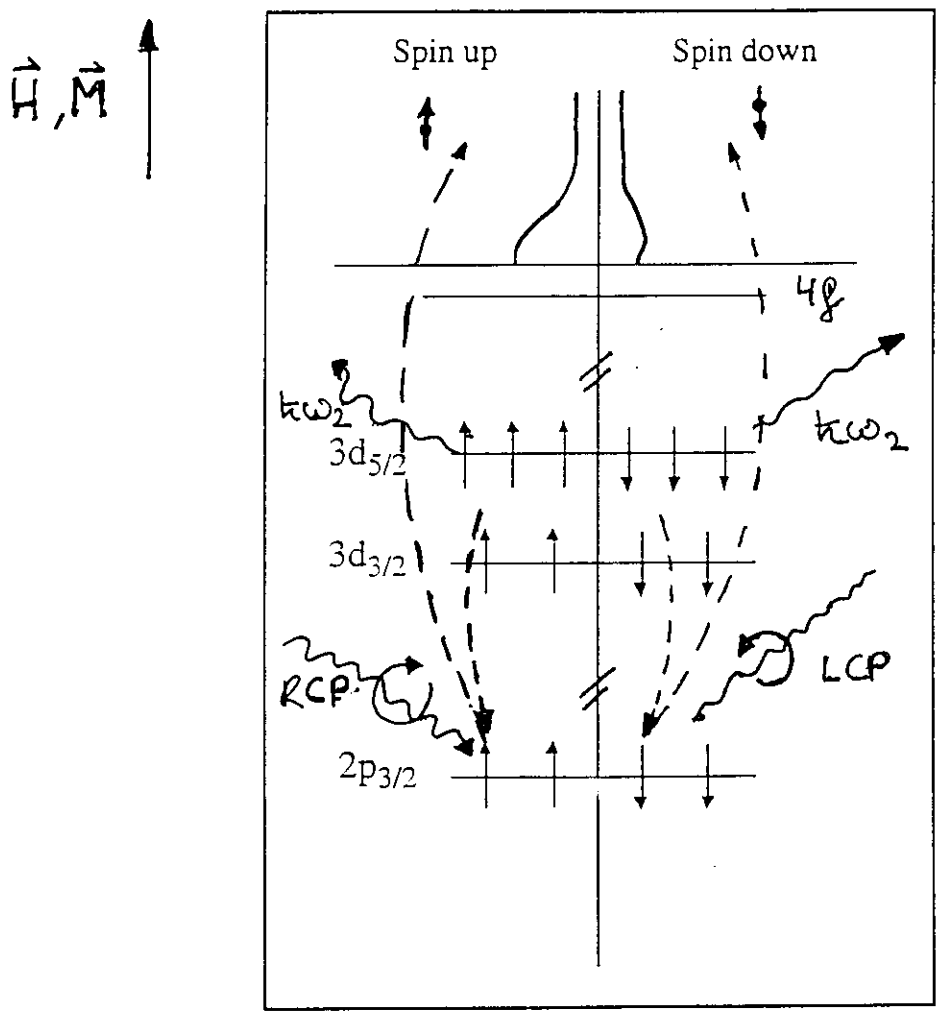


$$|F\rangle = |nd_{\downarrow}^{9}\, 4f_{\uparrow}^{7}\rangle$$ excitation of a spin-up electron

$$|F\rangle = |nd_{\uparrow}^{9}\, 4f_{\uparrow}^{7}\rangle$$ excitation of a spin-down electron

# RIXS excited with circular polarized x-rays

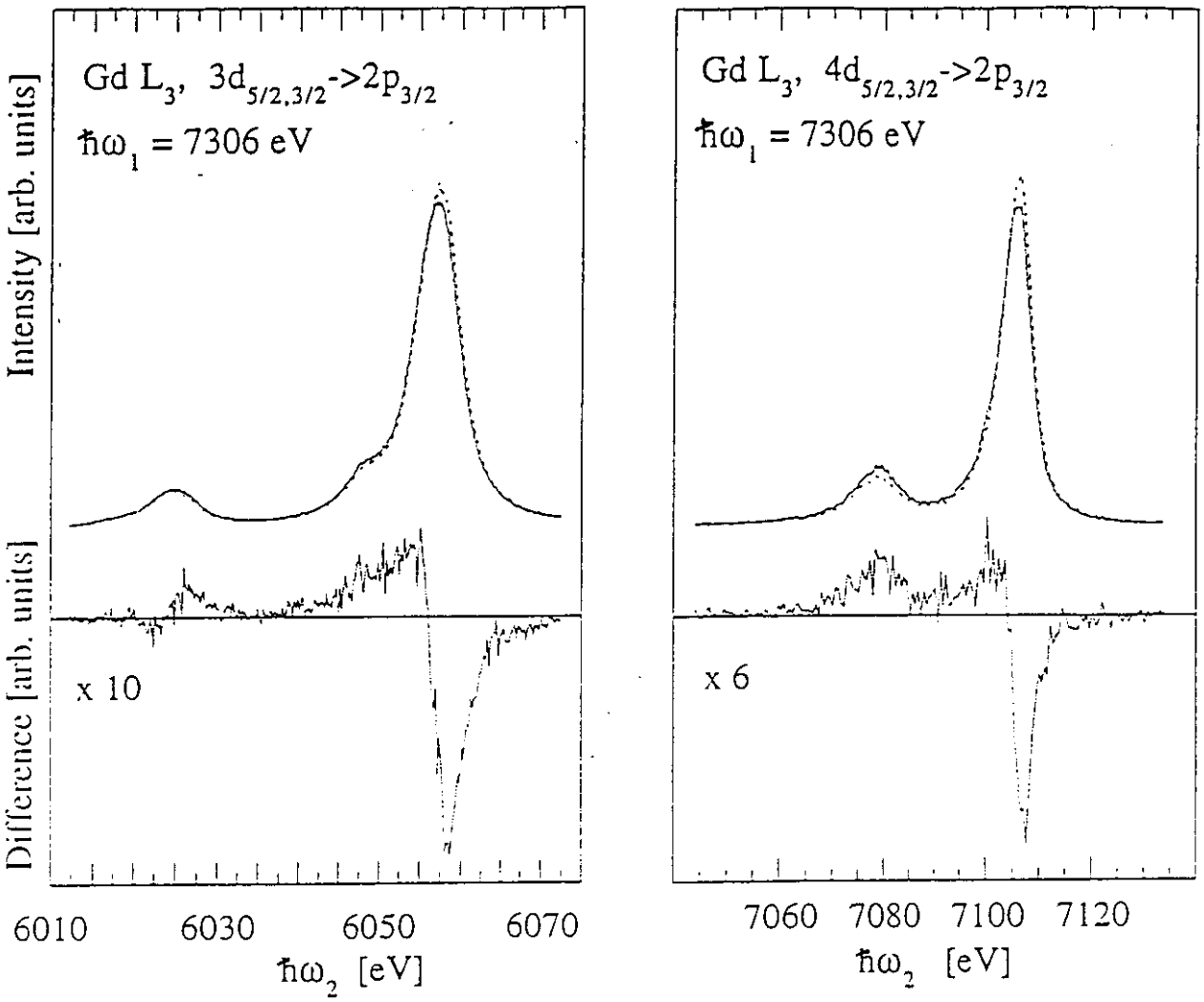


$2p_{3/2}$ Photoelectron polarization $P_e = \dfrac{[n(\uparrow\uparrow) - n(\uparrow\downarrow)]}{[n(\uparrow\uparrow) + n(\uparrow\downarrow)]} = 0.25$

Creation of a spin-polarized (deep) core-hole (2p)

Polarized (shallow) core-hole ($3d^9$, $4d^9$) : $^2D$

Polarized 4f-shell ($4f^7$) : $^8S$

Final State Symmetry : $^{7,9}D$

# Atomic Multiplet Calculations

- F.M.F. de Groot, M. Nakazawa, A. Kotani, M.H. Krisch, and F. Sette, Phys. Rev. B, in print

## 1) Lα - emission; $\zeta_{so} >> G_{ex}$ (jj-coupling)

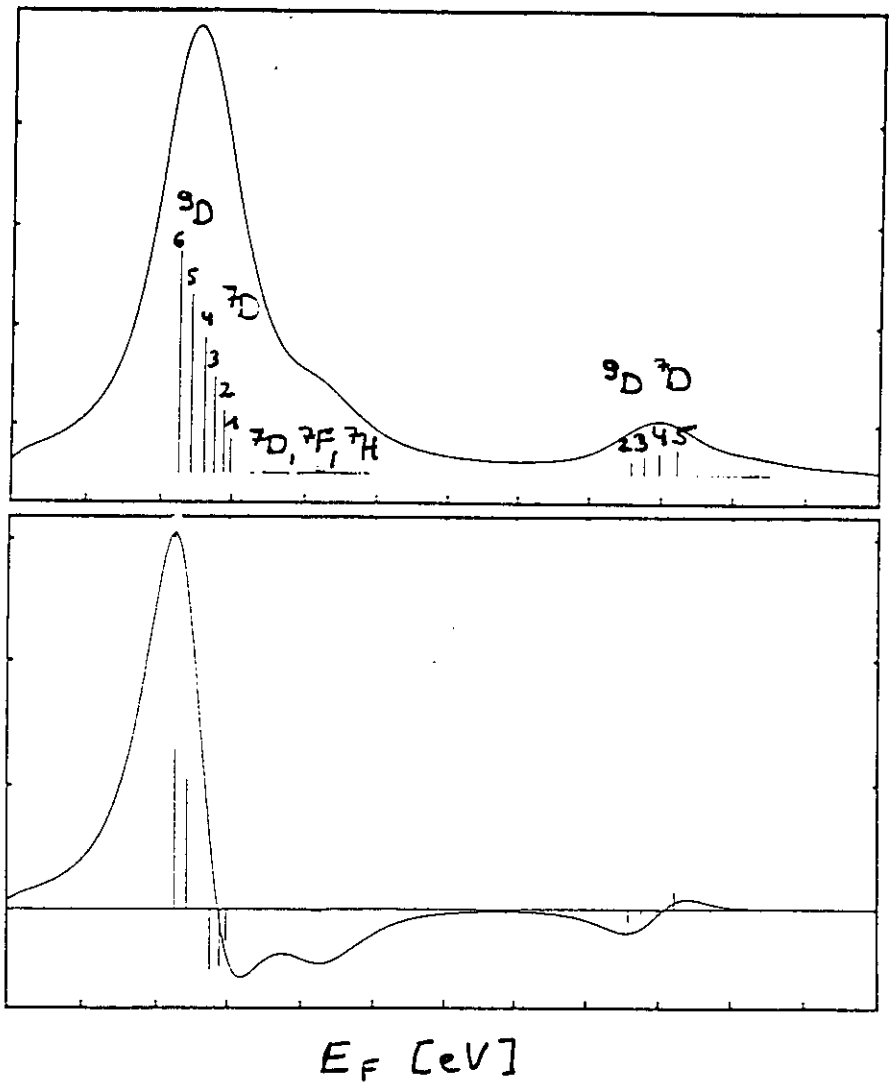


$j_{3d} = 5/2$

$^9D_6$ $S_{4f} \parallel S_{3d}$ => lowest final state energy, $(L \cdot S)_{3d} > 0$

⋮

$^7D_1$ $S_{4f} \nparallel S_{3d}$ => highest final state energy, $(L \cdot S)_{3d} > 0$

$j_{3d} = 3/2$

$^9D_2$ $S_{4f} \parallel S_{3d}$ => lowest final state energy, $(L \cdot S)_{3d} < 0$

⋮

$^7D_5$ $S_{4f} \nparallel S_{3d}$ => highest final state energy, $(L \cdot S)_{3d} < 0$

## 2) Lβ - emission; $\zeta_{so} < G_{ex}$ (LS-coupling)

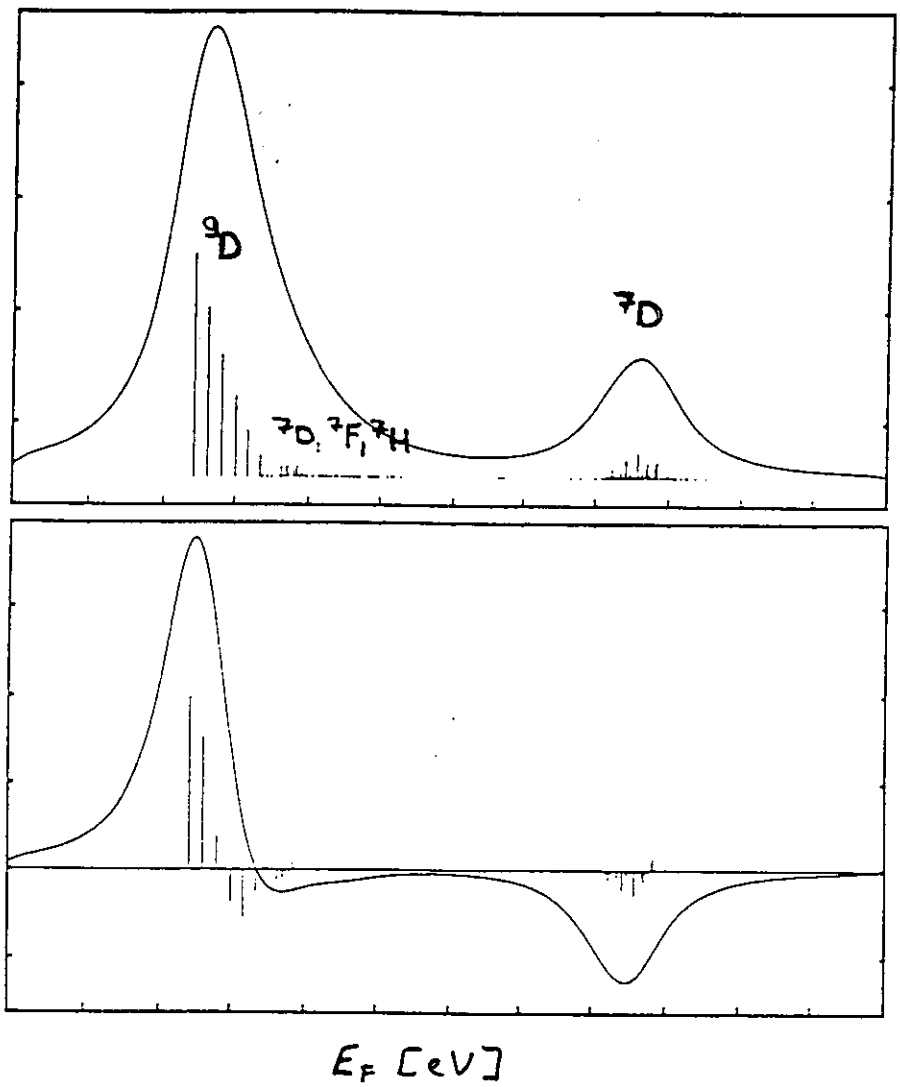


"High Spin"

$^9D_6$ $S_{4f} \parallel S_{3d}$ => lowest final state energy, $(L \cdot S)_{3d} > 0$

⋮

$^9D_2$ $S_{4f} \parallel S_{3d}$ => highest final state energy, $(L \cdot S)_{3d} < 0$

"Low Spin"

$^7D_1$ $S_{4f} \nparallel S_{3d}$ => lowest final state energy, $(L \cdot S)_{3d} \gtrless 0$

⋮

$^7D_5$ $S_{4f} \nparallel S_{3d}$ => highest final state energy, $(L \cdot S)_{3d} < 0$

# Valence Band Emission XMCD

• Probing the element- and symmetry specific spin polarizaton of the occupied density of states below the Fermi level.

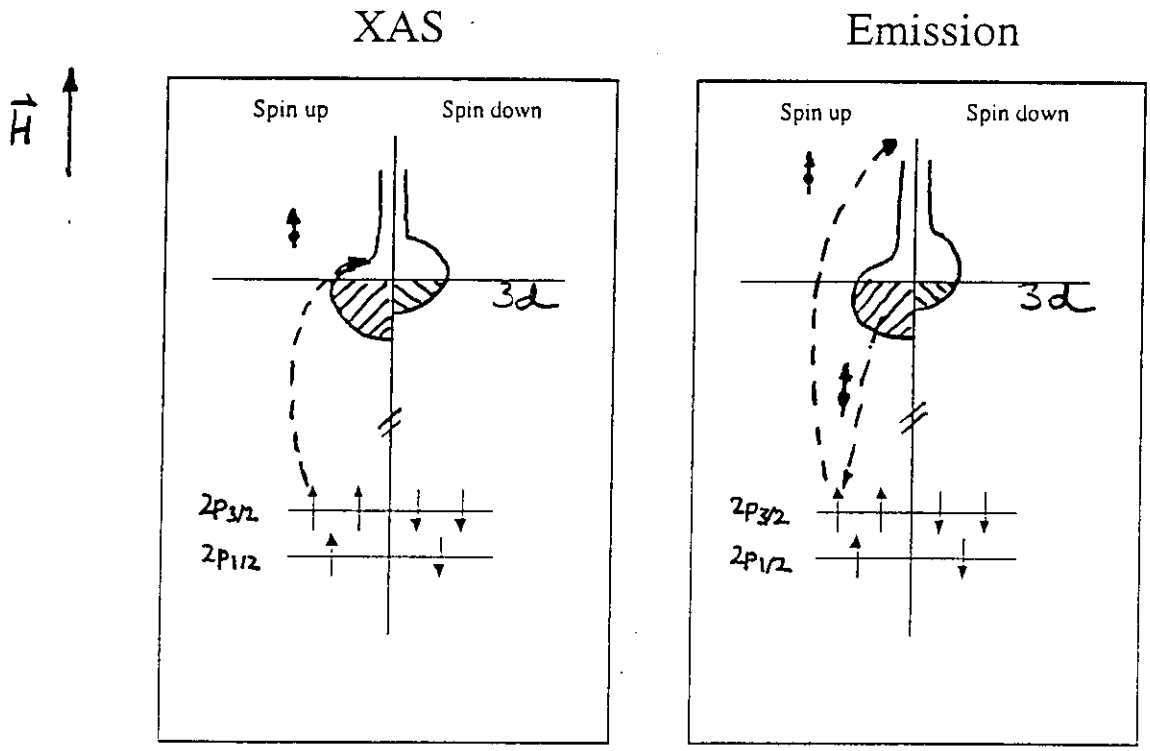


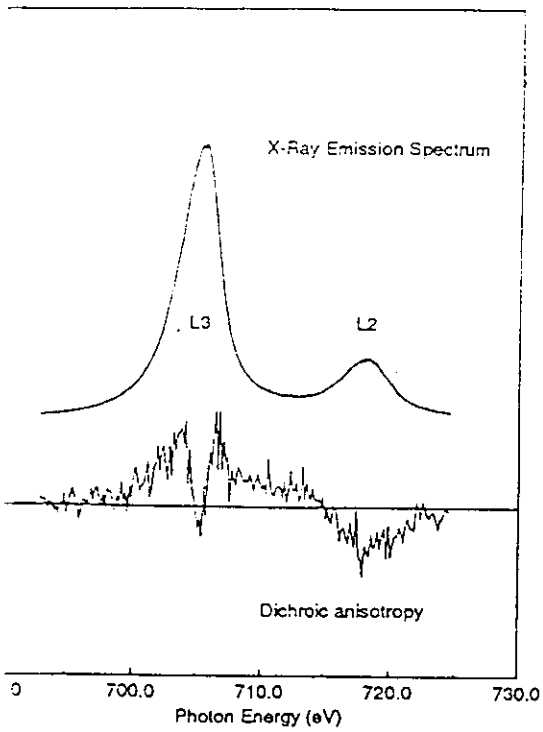


C.F. Hague et al.; PRB 48, 3560 (1993)

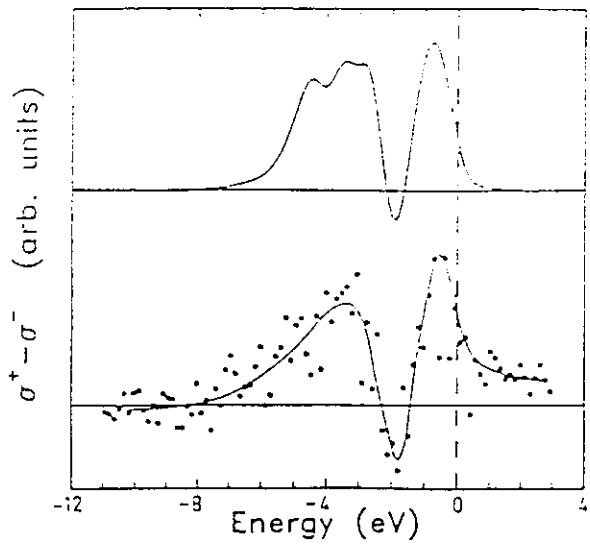


FIG. 2. The (normalized) Fe $L_3$ magnetic circular dichroism signal ($\sigma^+ - \sigma^-$): the upper curve is the theoretical prediction for $\omega_i$ equals threshold energy, folded with the experimental resolution function; the experimental result is given in the lower curve (the continuous line serves as a guide for the eye).

# Valence Band Emission from NiO

(C.C. Kao et al.; PRB 54, 16361 (1996)

• Resonant enhancement of the charge-transfer excitations

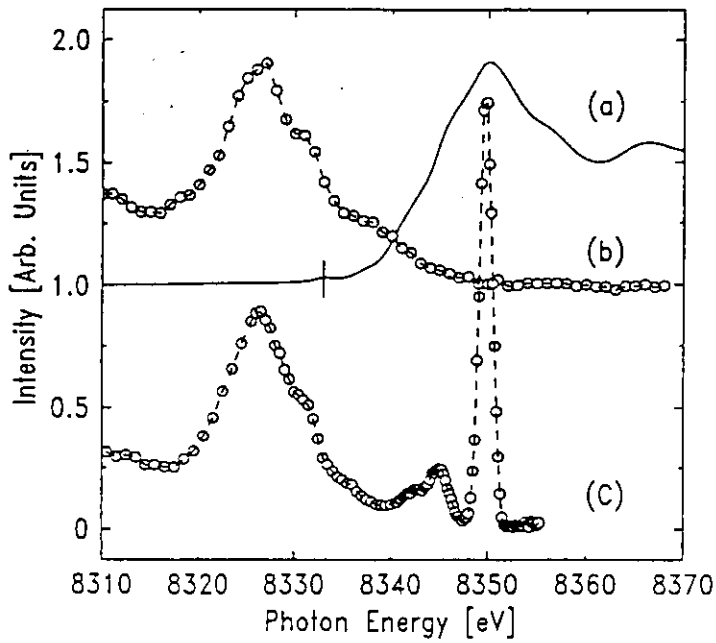


FIG. 1. (a) Ni $K$ absorption spectrum of NiO. (b) Normal valence-band x-ray-emission spectrum of NiO. (c) Resonant inelastic x-ray-scattering spectrum of NiO obtained with the incident photon energy tuned to the main peak of the absorption spectrum (a).

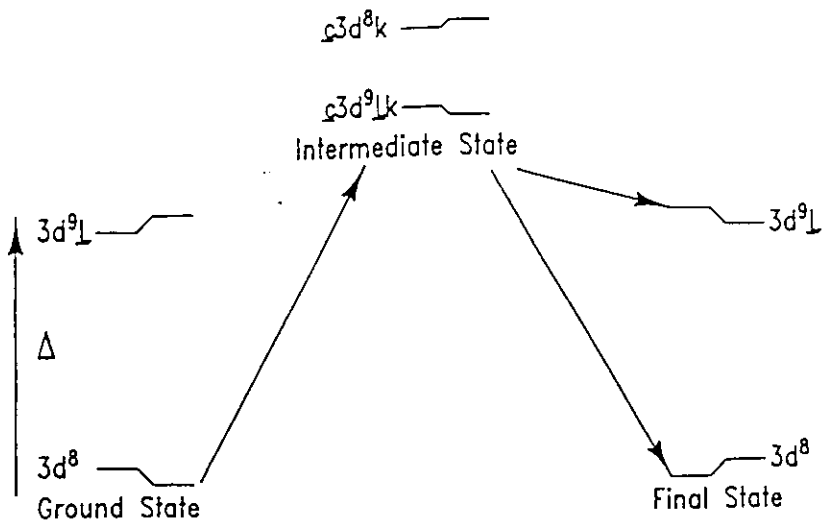


FIG. 4. Schematic energy-level diagrams of NiO in the ground state, the intermediate state, and the final state of the x-ray resonant Raman process.

# X-Ray Raman Scattering from low Z Materials

XAS

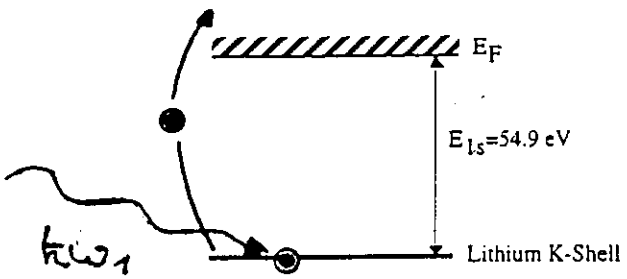


IXS

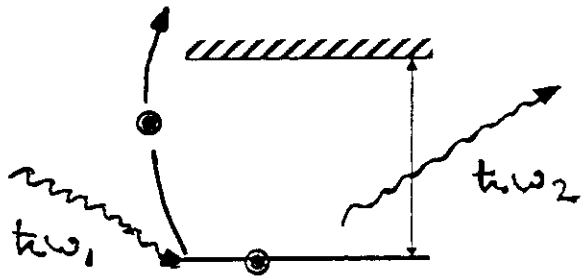


$E_b + \varepsilon = \hbar\omega_1$

$E_b + \varepsilon = \hbar\omega = \hbar\omega_1 - \hbar\omega_2$ .

$$\frac{d^2\sigma}{d\hbar\omega_2\, d\Omega} = r_o^2 \frac{\omega_2}{\omega_1}\left(\bar{e}_1\cdot\bar{e}_2\right) \sum_F \left|\left\langle F\left|\Sigma_j\, e^{i\bar{q}\bar{r}_j}\right|I\right\rangle\right|^2 \delta\left(E_F - E_I - \hbar\omega\right)$$

r is the radial extent of the core wave function under consideration

$qr << 1$: $e^{iqr} \approx 1+iqr$ .

Dipolar Regime: Identical to photon absorption, where $\bar{q}$ plays the role of the photon polarization vector $\bar{e}_1$.

(Mizuno and Ohmura, 1967)

$qr >> 1$: $e^{iqr}$ .

Multipolar Regime: quadrupolar and monopolar excitations

(Doniach, Platzman and Yue, (1971))

# Comparison between x-ray Raman Scattering and soft x-ray absorption

H. Nagasawa, S. Mourikis, and W. Schülke; J. Phys. Soc. Jpn. 58, 710 (1989)

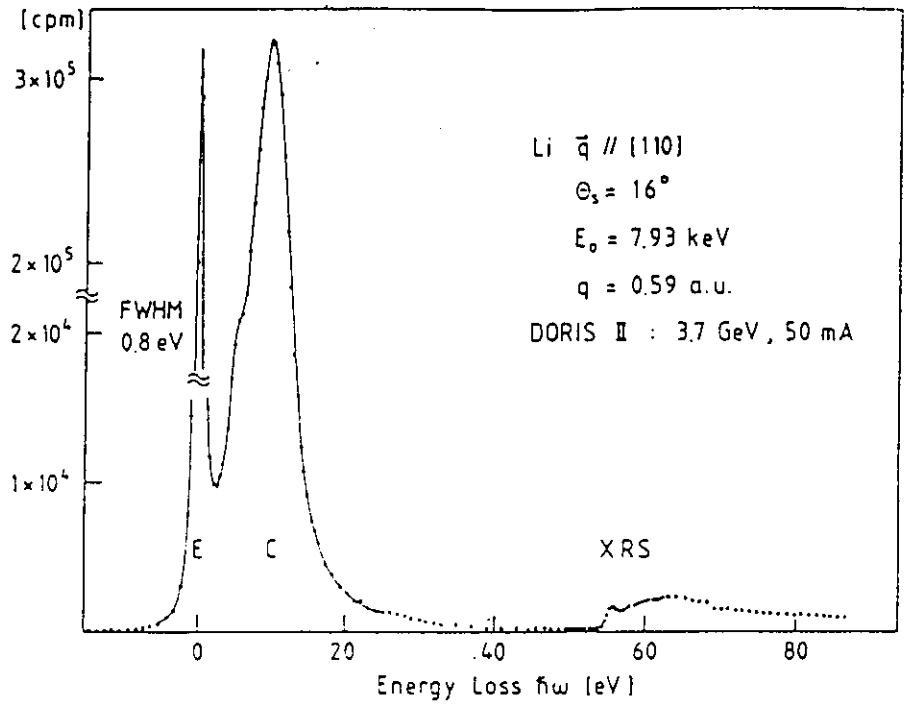


Fig. 1. Raw experimental data for Li single crystal obtained in the dispersion compensating case. The X-ray Raman spectrum (XRS) has an edge like onset at the binding energy of the Li $K$-electron of about 55 eV. E and C denote the quasielastically scattered Rayleigh line and the $S(q, \omega)$ profile from the valence electrons, respectively.

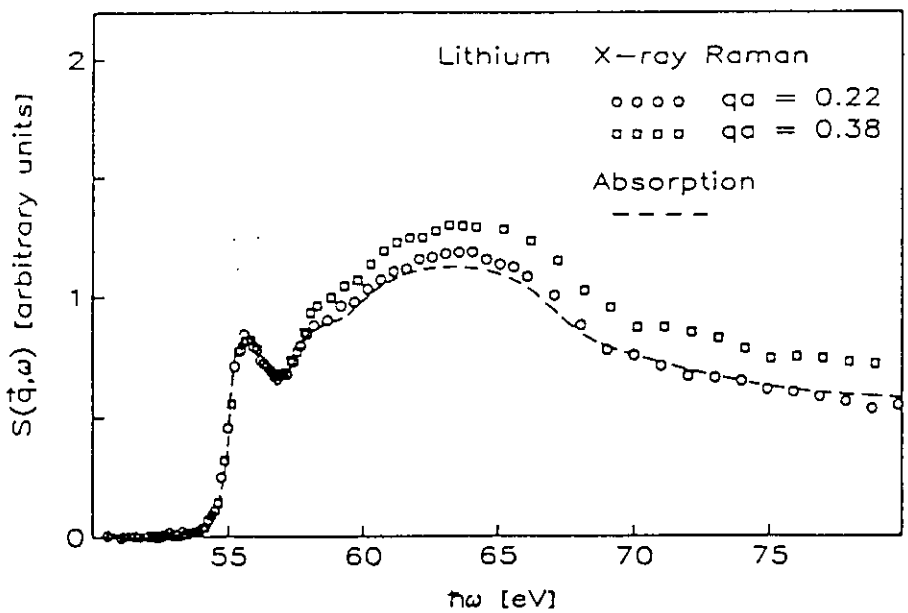


Fig. 5. Comparison of X-ray Raman spectrum (XRS) and soft X-ray absorption data for Li metal; circles: XRS for $qa=0.22$, squares: XRS for $qa=0.38$, dashed line: reduced soft X-ray absorption curve.

# Comparison of XRS- versus soft XAS-EXAFS

K. Tohji and Y. Udagawa; Phys. Rev. B 39, 7590 (1989)

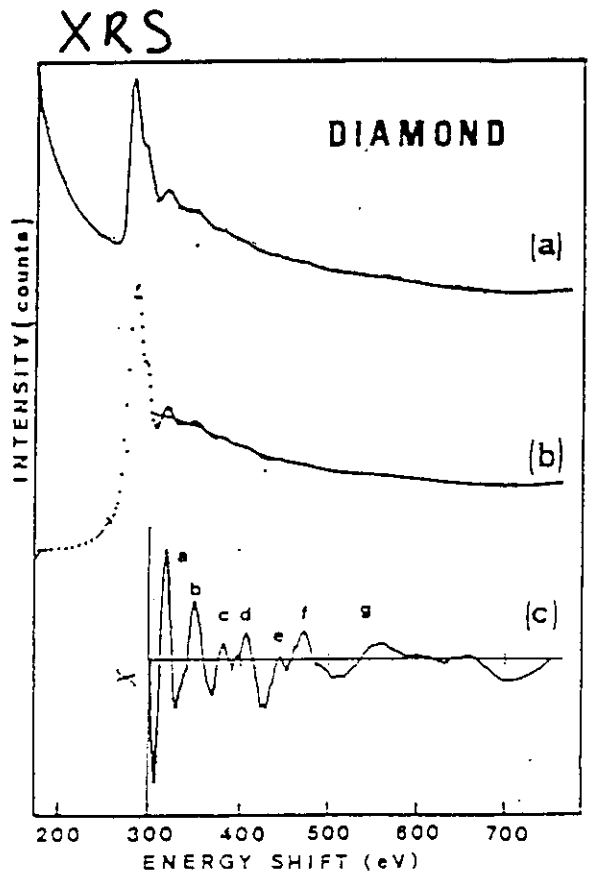


FIG. 3. (a) Part of the raw inelastic-scattering spectrum from diamond (dots) and the smoothed spectrum (solid line) observed at 60°. (b) Raman spectrum obtained from (a) by removing the Compton tail and the assumed smooth background. (c) Extracted oscillation from (b). Features (a)–(g) correspond to those in Fig. 4.

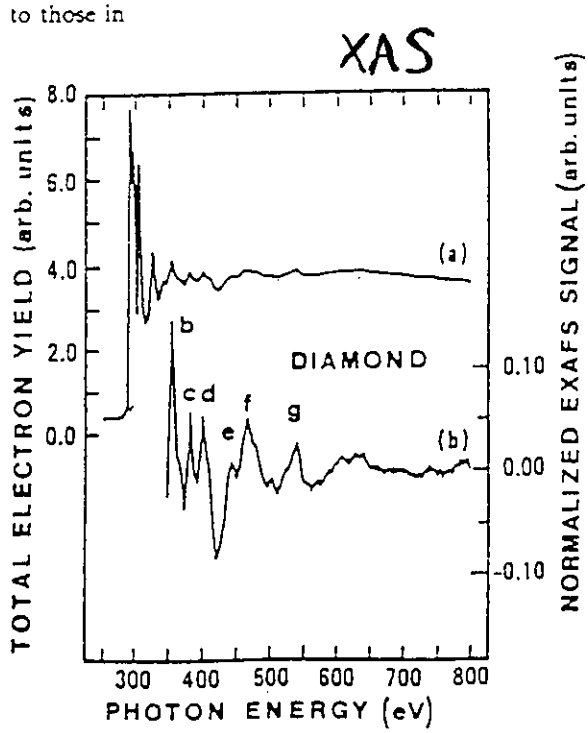

# Anisotropic x-ray Raman Spectra

H. Nagasawa, S. Mourikis, and W. Schülke; J. Phys. Soc. Jpn. 58, 710 (1989)

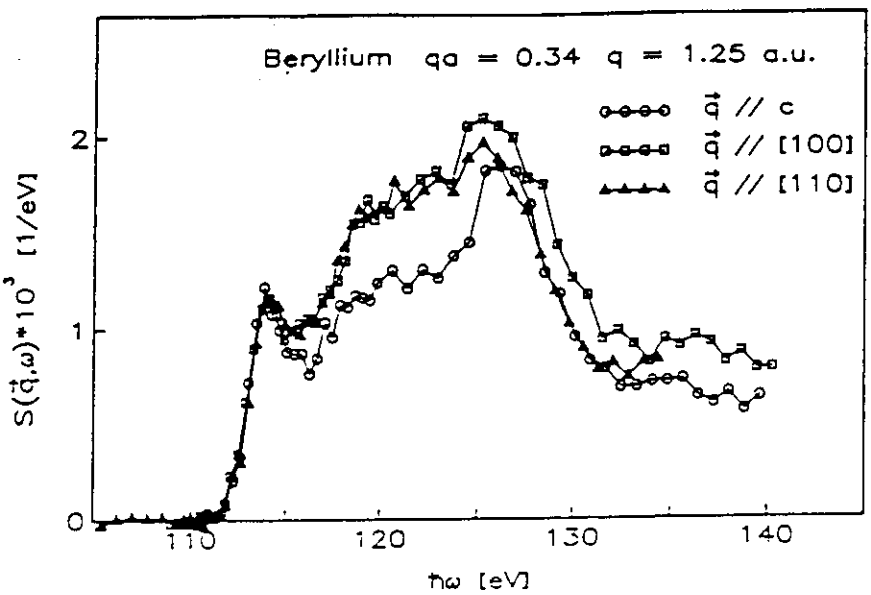


Fig. 3. Anisotropic Be X-ray Raman spectra for $q \parallel c$, $q \parallel [100]$ and $q \parallel [110]$. The dependence of the fine structure on the $q$-direction can be attributed to $q$-dependent symmetry projections off the density of unoccupied states.

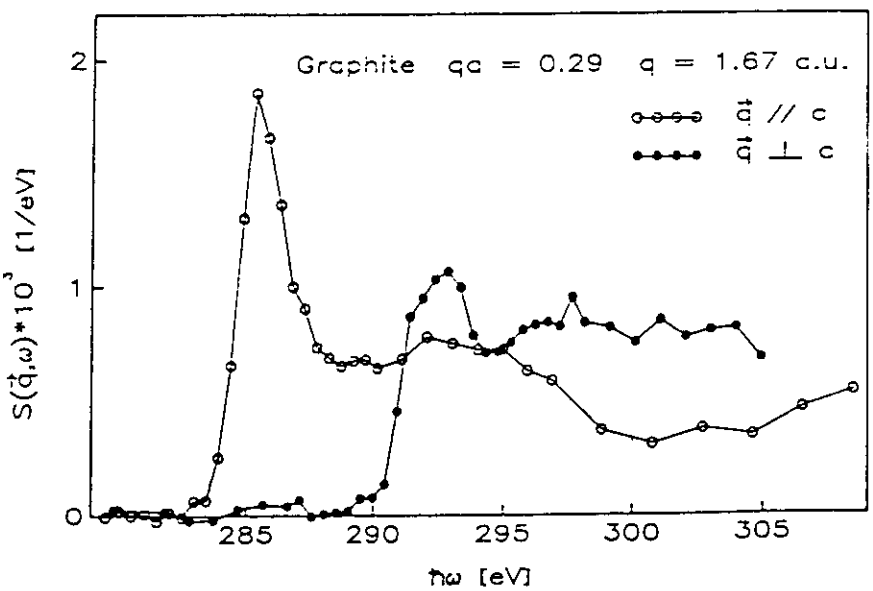


Fig. 4. The anisotropic graphite X-ray Raman spectra for $q \parallel c$ and $q \perp c$ reflect the density of carbon $\pi$-states and $\sigma$-states, respectively.

# IRS beyond the dipole selection rules at the Li K-edge

Sample: 12 mm lithium metal rod, kept at 10 K
Incident Energy: $\geq$ 9885 eV
Scattered energy: 9885 eV
Scattering angles: 10° and 150°

Momentum transfer $q \approx 2k_0 \sin(\theta_S/2)$
Radial extent of Li 1s wavefunction: 0.02 nm

$q(10°) = 8.7\ nm^{-1}$ $qr(10°) = 0.175$
$q(150°) = 97\ nm^{-1}$ $qr(150°) = 1.93$

Total energy resolution $\Delta E$: 1.6 eV or 80 meV

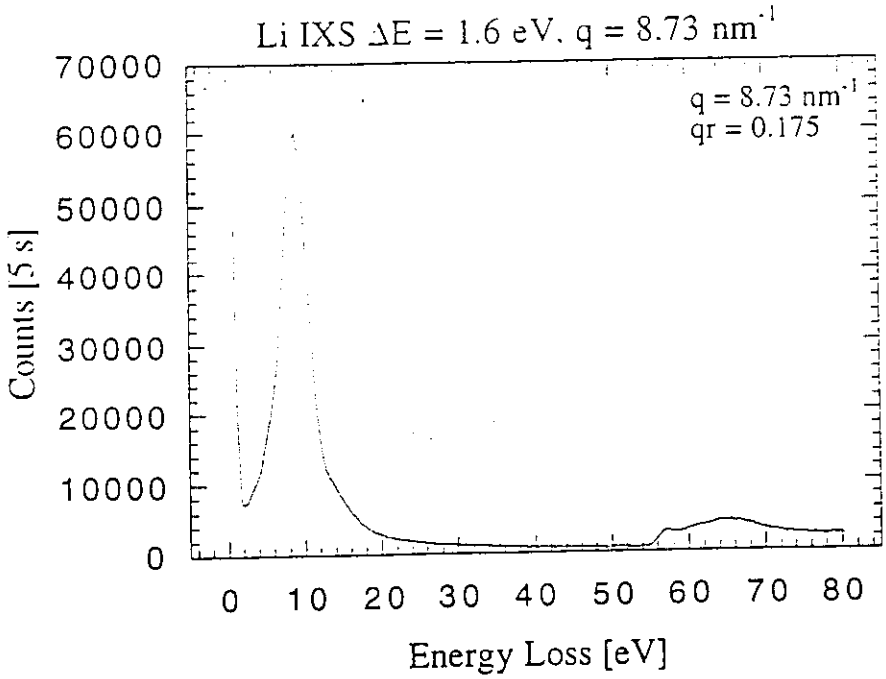

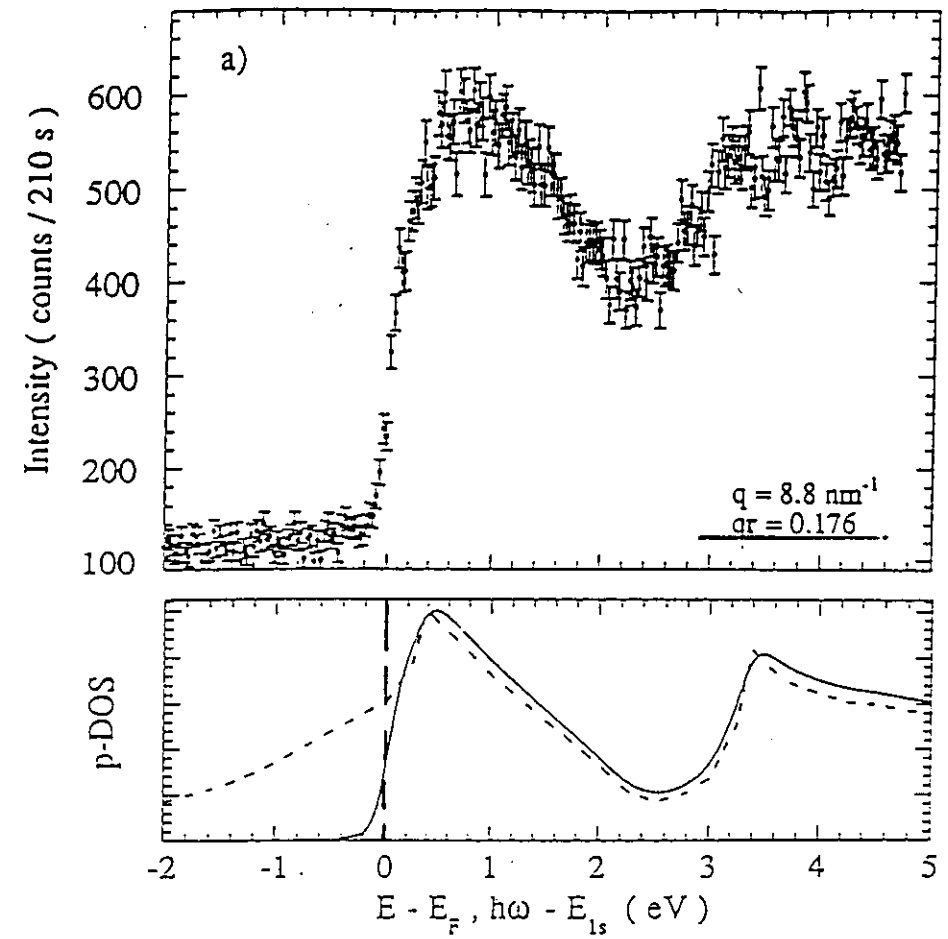
a)
Intensity ( counts / 210 s )
600
500
400
300
200
100
q = 8.8 nm$^{-1}$
qr = 0.176
p-DOS
-2
-1
0
1
2
3
4
5
E - E$_F$ , hω - E$_{1s}$ ( eV )

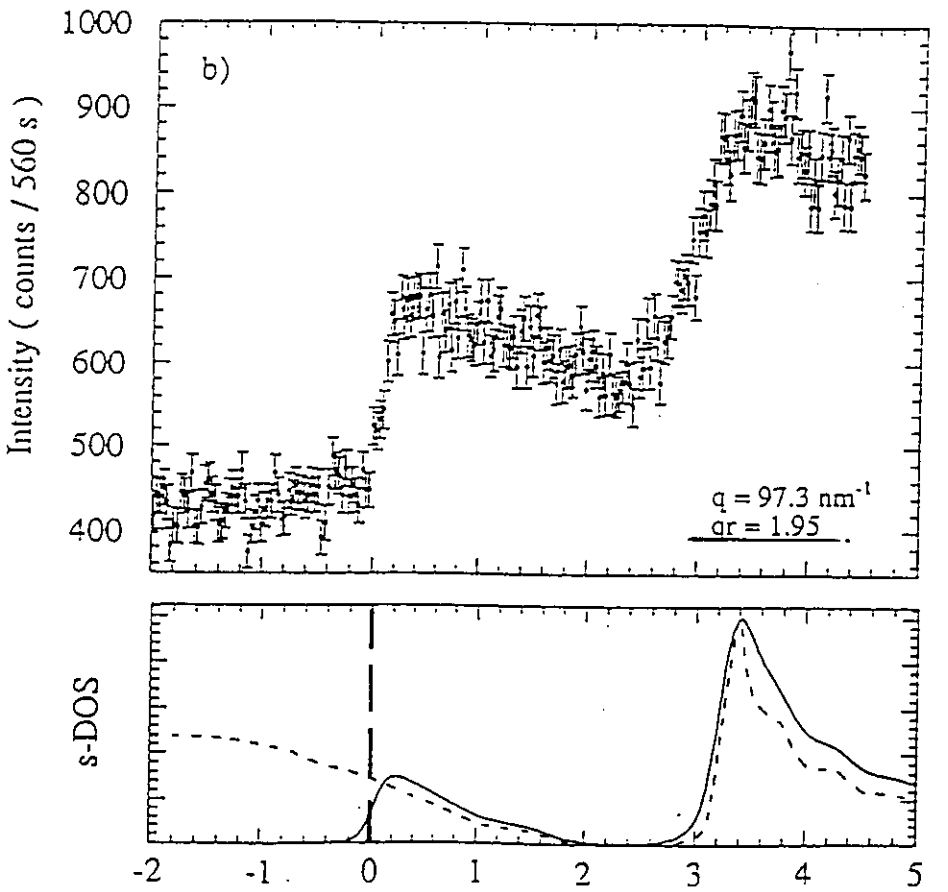
b)
Intensity ( counts / 560 s )
1000
900
800
700
600
500
400
q = 97.3 nm$^{-1}$
qr = 1.95
s-DOS
-2
-1
0
1
2
3
4
5

## Li K-edge Absorption

- H. Petersen; Phys. Rev. Lett. 35, 1363 (1975)

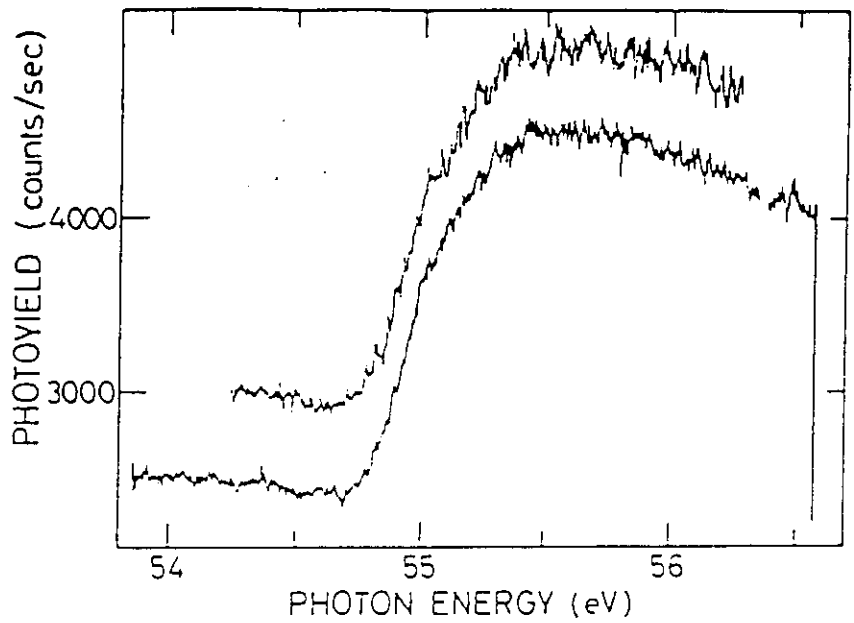


## Li K-edge Electron Energy Loss Spectroscopy

- J.J. Ritsko et al.; Phys. Rev. B 10, 5017 (1974)

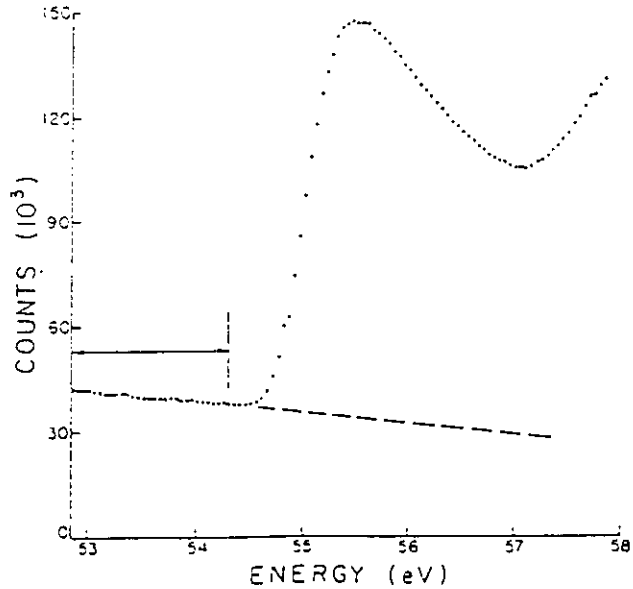

# Summary

## Resonant IXS:

- Useful (Powerful) complement to other core spectroscopies.

  - Isolation of overlapping excitation channels, not visible in XAS (RIXS for the interpretation of XMCD data)

  - Use of circular polarized x-rays

    - Study of electron correlation effects, similar to XPS, but bulk sensitive (Spectral moment analysis)

    - Probing the spin-resolved occupied density of states

  - Probing the spin-resolved empty density of states in systems without long range magnetic order (Paramagnets. Antiferromagnets)

## IXS from core levels of low Z- materials:

Soft XAS in the hard X-ray regime:
- experiments under extreme conditions such as high temperature, high pressure.

Exploitation of excitations beyond the dipole selection rule.